Multi-site rate control analysis identifies ribosomal scanning as the sole high-capacity/low-flux-control step in mRNA translation

Helena Firczuk[1], James Teahan[1], Pedro Mendes[2] and John EG McCarthy[1]

[1]Warwick Integrative Synthetic Biology Centre [WISB] and School of Life Sciences, University of Warwick, Gibbet Hill, Coventry CV4 7AL, UK
[2]Center for Quantitative Medicine, UConn Health, 263 Farmington Avenue, Farmington, CT 06030-6033, USA.

Running title: Ribosomal scanning as a low-flux-control step

Keywords: protein synthesis; rate control; ribosomal scanning; polypeptide initiation; yeast

Abbreviations
CuRE, copper-responsive regulatory element; DEAD box proteins contain the motif Asp-Glu-Ala-Asp; MFC, multi-factor complex; R_1^J, response coefficiant for protein synthesis as a function of intracellular translation factor abundance in the near-physiological range; SBGN, Systems Biology Graphical Notation.

Correspondence

John E.G.McCarthy
School of Life Sciences
University of Warwick
Gibbet Hill Campus
Coventry CV4 7AL
UK

Tel.: (0044) 7793 413673

Email: john.mccarthy@warwick.ac.uk

Abstract

Control of complex intracellular pathways such as protein synthesis is critical to organism survival, but is poorly understood. Translation of a reading frame on eukaryotic mRNA is preceded by a scanning process in which a subset of translation factors helps guide ribosomes to the start codon. Here, we perform comparative analysis of the control status of this scanning step that sits between recruitment of the small ribosomal subunit to the m^7GpppG-capped 5'end of mRNA and of the control exerted by downstream phases of polypeptide initiation, elongation and termination. We have utilised a detailed predictive model as guidance for designing quantitative experimental interrogation of control in the yeast translation initiation pathway. We have built a synthetic orthogonal copper-responsive regulatory promoter (P_{CuR3}) that is used here together with the *tet07* regulatory system in a novel dual-site *in vivo* rate control analysis strategy. Combining this two-site strategy with calibrated mass spectrometry to determine translation factor abundance values, we have tested model-based predictions of rate control properties of the *in vivo* system. We conclude from the results that the components of the translation machinery that promote scanning collectively function as a low-flux-control system with a capacity to transfer ribosomes into the core process of polypeptide production that exceeds the respective capacities of the steps of polypeptide initiation, elongation and termination. In contrast, the step immediately prior to scanning, i.e. ribosome recruitment via the mRNA 5'cap-binding complex, is a high-flux-control step.

Introduction

Biological systems are generally highly complex and subject to multilayered control that can only be elucidated with the help of a combination of experimentation and computational modeling. The integration of multiple levels of system architecture generates higher-order functionalities and/or emergent properties that cannot be deduced by simple extrapolation from the properties of the system components [1]. A prime example of a complex biomolecular system is the protein synthesis machinery, which is ultimately responsible for creating all of the structures and functions that are associated with living cells [2-4]. Maintaining an efficient, high-precision mRNA translation machinery represents a major logistical and energetic burden for the cell, to the extent that, in the case of yeast, at least 76% of its total cellular energy budget is estimated to be committed to protein synthesis [5]. In addition, this machinery needs to be capable of accurate regulatory responses to environmental change [6]. At the heart of these key properties are features of control that are only beginning to be understood.

The translation pathway is thought to involve the progressive stoichiometric assembly [and disassembly] of multiple intermediate complexes (as shown for the scanning/initiation steps in Fig. 1A,B). Unexpectedly, we discovered previously that the intracellular abundance of the participating translation factors varies over at least a twenty-fold range [7], despite the fact that the inter-subunit stoichiometries in the complexes are generally unity (Fig. 1B). The exact number of formally recognized translation factors depends on the criteria used to define them, but it is generally agreed to be approximately twenty [7]. These proteins assist the ribosomes in multiple ways, manifesting a range of properties and functionalities, including: ATP/GTP hydrolysis or guanine nucleotide exchange [3,8-10], remodeling of ribonucleoprotein complexes [11,12], promoting specific intermolecular interactions (involving targets that include the m^7Gppp cap [13], sites on the ribosome [2], tRNAs [2,3], and other translation factors [14,15]), and molecular mimicry [15]. Systems Biology Graphical Notation (SBGN [16]) diagrams help to illustrate what we know about the roles of the respective factors and the relationships between them (Fig. 2). These diagrams also evince the complexity of a molecular machinery over which the cell must exercise precise control in order to ensure viability.

Eukaryotic translation depends upon recruitment of (5'-capped) mRNA to the ribosomal 43S complex (comprising the 40S subunit plus the Multi-Factor-Complex (MFC) factors eIF1, Met-tRNA^{Met}.eIF2.GTP, eIF3 and eIF5, together with eIF1A) in a step mediated by the cap-binding complex, which in its minimal form comprises the cap-binding protein eIF4E and eIF4G [17]. It is thought that the DEAD-box helicase eIF4A is also part of the cap-binding complex eIF4F, although it is, in itself, a poor RNA helicase that depends on interactions with other factors for its full functionality [18,19]. Moreover, interactions between eIF4G and the poly[A]binding protein Pab1 are capable of mediating interactions between the 5' and 3' ends of mRNA [20], whereby Pab1 stimulates both translation initiation [21,22] and deadenylation by the Pan2/Pan3 complex [23]. Scanning of the 5' untranslated region (5'UTR) by the 40S subunit is facilitated by translation factors that individually have been found to exercise very limited influence on rate control (these include eIF1, eIF3 and eIF5, all of which manifest very low steady-state rate control (R_1^J) values; [7]). There is a further essential DEAD-box helicase, called Ded1, that can associate with the cytoplasmic (and nuclear) cap-binding complex [24,25]. This protein promotes the steps of scanning and polypeptide initiation, particularly on long 5'UTRs, but the mechanism of its action is unclear [26]. The progression of 40S ribosomal subunits along the mRNA during scanning is generally not dependent on specific recognition of nucleotides, and can be simulated using a partially random walk type of model [26]. Specific recognition steps are, however, required to initiate scanning (5'cap recognition mediated by eIF4E) and to enable polypeptide initiation (start codon recognition mediated by initiator-tRNA in the ribosomal P site).

Once the polypeptide encoded by the main open reading frame has been initiated, the eukaryotic elongation factors take over. The elongation factor eEF1A delivers aminoacylated tRNAs (aatRNAs) to the ribosomal acceptor (A) site, while the eEF1B complex (comprising subunits α and β in yeast) promotes guanine nucleotide exchange on eEF1A [9]. eEF2, on the other hand, is a GTP-dependent translocase that is responsible for the movement of nascent peptidyl-tRNAs from the A-site to the P-site on the ribosome [3]. Deacylated tRNAs are released from the ribosomal exit (E) site in a process that in yeast (but not animals or plants) is promoted by eEF3 [27]. Uncharged tRNAs are recharged with the corresponding amino acids in preparation for another round of incorporation. Finally, polypeptide termination is triggered by the termination

factor eRF1 upon recognition of a stop codon, whereby eRF1 is supported by eRF3, which has a ribosome-dependent and eRF1-dependent GTPase activity [15].

Given that protein synthesis is ultimately the source of all cellular structures and processes, and thus is of intrinsic importance to cell viability and selective competitiveness, research to characterize the principles of control in the translation machinery remains a major priority. We still do not understand, in precise terms, how interactions between the assemblage of translation machinery components determine the rate of protein synthesis, relationships that are of course fundamental to the regulatory responses of this system [28]. A particularly distinctive feature of eukaryotic translation, compared to its prokaryotic counterpart, is the scanning process that links ribosomal recruitment of mRNAs via the 5'end to polypeptide initiation at a start codon further along in the nucleotide sequence. Our earlier work [7] raised the possibility that the activities of the components supporting the scanning step in translation may be set at levels that could render their contributions less rate-controlling than those of other factors. Clarification of rate control distribution in the translation machinery is critical to developing an understanding of the evolution of this important system. It is tempting to make *a priori* assumptions about the contributions of what are commonly referred to as 'rate-limiting' steps to the overall control of translation. However, the nature of rate control in such a complex system can only be elucidated on the basis of quantitative experimental rate control analysis. Moreover, all of the translation factors act interactively as part of the overall translation machinery, and therefore it is essential that we examine the influence of combined multi-site control modulations.

Here, we employ a novel dual-site *in vivo* rate modulation strategy that has been designed to test the validity of hypotheses concerning control in such a complex molecular machinery. We use it to develop a wider picture of rate control in the scanning step as a whole, using yeast as a model system. This work also demonstrates that the combination of *in vivo* multi-site rate control analysis with computational modeling is a broadly applicable strategy for elucidating control principles governing complex intracellular machineries, one that can be expected to contribute to the important wider goal of developing a meaningful *in silico* representation of at least the core processes of the living cell.

Results

Testable predictions of rate control based on a highly parameterised computational model

The complexity of the translation machinery makes it necessary to utilize computational modeling as a tool to help develop understanding of the rate control characteristics of this system. Our earlier work on the impact of changes in the abundance of individual translation factors on the translation process *in vivo* suggested that many of the factors associated with scanning exert minimal rate control when present at an abundance close to that of a wild-type cell [7]. This raises important questions about how scanning as an overall process contributes to the control of global protein synthesis. Here, we have utilized an establshed computational model [7] to provide more detailed (testable) predictions that can be used to help build a reliable picture of the distribution of control over the respective stages of protein synthesis. It is essential to use a model that is capable of reproducing the interdependence between the respective phases of translation. A key factor in determining our choice of this particular model is that it is highly detailed with regard to the mRNA recruitment and scanning steps. On the other hand, the coding region comprises a minimalized length of 20 codons, thus keeping calculation times within reasonable limits. Our strategy for using the model is to examine the predicted impact of the pairwise modulation of the intracellular abundance translation factors, since this represents a challenging test of the model's ability to simulate complex system behavior. At the same time, it is important to note that this model was refined on the basis of fitting to single factor modulation data [7] and has been used here to provide indications of expected rate-activity relationships rather than accurate predictions of the results of dual-factor modulation experiments.

This approach is exemplified by model outputs for the reciprocal relationship between the activities of eIF1 and eIF5 (Figs. 3A and 4A). In each case, the translation rate is plotted against the intracellular abundance of one of the pair of factors over a range of different pre-determined abundance values for the second factor. A striking feature of these model outcomes is the appearance of a plateau in the dependence of translation rate on abundance in the region near the physiological 100% [wild-type] value. Such a plateau signifies marked insensitivity of the translation rate to changes in translation factor abundance, as would be expected if the factor has excess capacity in the near-physiological concentration range. In the case of eIF1 and eIF5, reduction in

the abundance of the second factor (for example, eIF1 in Fig. 3A; eIF5 in Fig. 4A) leads to a progressive loss of the plateau. At even lower abundance values of the second factor (below approximately 80%), the 'titrated' first factor of the pair shows significant predicted rate control sensitivity at any abundance below 100% (see red lines in Figs. 3A and 4A). The response relationship of translation rate to abundance changes for eIF1 and eIF5 in this region below 80% suggests that the contributions of eIF1 and eIF5 (to positioning of the initiator met-tRNA in the ribosomal 40S subunit to enable successful scanning) are mutually additive.

We next compared the interdependence of rate control behaviour predicted for the translation factor pair eIF1 and Pab1. The latter protein plays a role in promoting recruitment of capped mRNAs (via the cap-binding complex, and potentially also via the bridging complex between the cap-binding complex and the mRNA 3' end). In this case, the model predicts that both factors manifest very low rate-sensitivity in the near-physiological abundance range over a wide range of abundance values for the second factor in the pair. Indeed, the extent of the plateau increases as the abundance of the second factor (Pab1 in Fig. 3B; compare Pab1-related rate sensitivity at different levels of eIF1 in Fig. 4B) is decreased. In other words, in marked contrast to the predicted relationship between eIF1 and eIF5, eIF1 and Pab1 are predicted to act upon the global translation rate via independent routes, whereby if one factor is subject to limitation this imposes a reduced minimum requirement [saturation threshold] to achieve maximal pathway flux for the other.

We also performed modelling analysis of other scanning factor pairs in order to determine whether they are also predicted to manifest a similar pattern of minimal flux control in the near physiological range (Fig. 5). In the examples shown, we see that the outputs from the model for eIF3/eIF1 and eIF1A/eIF1 again predict pronounced rate insensitivity to variations in intracellular factor abundance at points close to 100% of the wild-type level. Indeed, this distinctive rate control behavior is generally predicted for the scanning translation factors, including those that comprise the MFC (Fig. 1B). In the next part of our work, we developed and implemented a novel experimental dual-site 'titration' strategy that enables us to test such model-derived predictions related to the interdependence of rate control by distinct factors.

A synthetic dual-site regulatory system for rate control analysis

Rigorous *in vivo* experimental analysis of gene expression control requires suitably engineered orthogonally acting tools that work (progressively) within a suitable range. However, there is a marked paucity of negative regulatory promoters for use in yeast that can be precisely regulated and act orthogonally (i.e. in a way that does not interfere with metabolic or genetic processes that are not directly linked to the targeted gene). Therefore, for this study, we set out to develop a new synthetic regulatory promoter that could be applied in parallel to the *tet07* regulatory system (Fig. 6A-C). More specifically, we needed to be able to apply progressively variable modulation of the activities of pairs of translation factors, since this would facilitate direct testing of predictions derived from our computational model. The approach described here is in certain respects analogous to the systematic use of targeted dual-gene mutation [29]. However, our approach explores the more precisely controllable impact of the simultaneous progressive modulation of two gene expression rates rather than interactions between genetic modifications. Moreover, in designing our dual-site regulatory system, we have ensured that progressive control can be applied in a way that allows us to study the effects of perturbations that impose only minimal deviations from the normal cellular state.

The *tet07* regulatory system has proved to be a reliable orthogonal tool for analysis of rate control ([7]; Fig. 6D]. As the starting point for a second, complementary regulatory system, we utilized the yeast P_{CTR1} promoter, whose activity is modulated in response to changes in the concentration of copper [30]. We constructed derivatives of this promoter in which we had inserted additional copper regulatory elements (CuRE elements; Fig. 6A). We looked for a combination of dynamic range of regulation and maximum achievable level of transcription that would complement the regulatory characteristics of the *tet07* regulatory system [31]. This was achieved using three CuRE elements (P_{CuR3}), which maximized the non-repressed activity of the promoter while maintaining the same dynamic range as wild-type P_{CTR1}. In further experiments, we established that the full dynamic range of the synthetic P_{CuR3} promoter could be explored using copper concentrations that were entirely non-toxic to *S.cerevisiae* (Fig. 7). The addition of further CuRE sequences (as illustrated by P_{CuR4} in Fig. 6C) did not provide any improvement in terms of

behavioural properties (Fig. 6B). We therefore used the synthetic promoter P_{CuR3} (Fig. 7A) in the dual site regulatory experiments described in this study.

Dual-site analysis of rate control in scanning

In reciprocal 'genetic titration' experiments, we have explored the rate control curves for eIF1 at different set abundances of eIF5, and *vice versa*. Both of these factors are involved in the scanning process [2]. Importantly, quantitation of the respective down-regulated translation factors was achieved using standardised mass spectrometry in a strategy that allowed us to perform simultaneous control measurements on the other translation factors (Fig. 8A,B). The results demonstrate down-regulation of translation factor activities (here evident as reduced protein abundance levels) corresponding to the genes placed under the control of the P_{CuR3} and *tetO7*-regulated promoters. Taking into account the expected accuracy intrinsic to the mass spectrometric procedure, it is evident that the endogenous abundance values for the non-regulated factors were minimally affected. These results confirmed the specificity of the targeted regulatory changes brought about using genomic constructs transcribed from the P_{CuR3} and *tetO7*-regulated promoters. At the same time we note that, as the expression of each gene encoding a translation factor is inhibited, global protein synthesis is, to differing degrees, also inhibited. Overall, therefore, in each experiment there is specific partial suppression of a selected translation factor relative to the other translation factors, accompanied by a reduction in the rate at which cells are formed. Further examples of the mass spectrometry outputs from other dual-site analysis experiments are given in Fig. 8C-H.

In this context it is important to note recent work indicating that eIF5 and eIF1 influence the stringency of start codon selection in mammalian cells [32]. Discrimination against poor AUG context, albeit of a relatively mild degree, has also been observed for eIF1 in yeast [33]. This might explain the limited degree of interdependence between abundance we have observed for eIF1 and eIF5 (Fig. 8A,B). At the same time, the striking feature of our experimental data is that the R_1^J value for eIF5 was unchanged within the 60%-100% relative abundance range of eIF1, and slightly increased at 50% of the wild-type eIF1 abundance (Fig. 3C), while, in the mirror experiment, the very low response coefficient (R_1^J) of eIF1 in the near-physiological abundance range (80% - 100%

of wild-type abundance) of this factor remained unchanged at all concentration levels of eIF5 tested (from 40% up to 100% of the wild-type abundance (Fig. 4C). We have calculated flux control coefficients for these respective dual modulation experiments and these are presented in the Supplementary Data section. If we now compare the experimental data with the predictions from the computational model (Figs. 3A and 4A), we find that the model predicts low rate-control sensitivity in the near-physiological range for each of this pair of factors only in the presence of an abundance of the other factor that exceeds 80% of the physiological level. Below 80%, the model predicts full additivity between the rate control impacts of eIF1 and eIF5 (red lines in Figs. 3A and 4A). Thus the general form of the experimental curves is correctly predicted by the model, but the point at which increased rate-control sensitivity for the 'titrated' factor in this pair becomes evident is shifted to a lower abundance level of the second factor.

Pab1 has been categorized as a multifunctional protein that is not dedicated to the translation process alone. It is not only thought to facilitate interactions between the 5' and 3' ends of mRNP molecules (via its interaction with eIF4G; 20,21) but is also believed to modulate deadenylation via its interactions with the Pan2-Pan3 complex [23]. Indeed, whereas reductions in the respective activities of eIF1 and eIF5 are tightly coupled to proportionate suppression of both global protein synthesis rate and growth, progressive diminution of Pab1 abundance has a more marked effect on growth than on global translation rate [7]. However, Pab1 belongs to the group of low R_1^J translation factors [7], and we sought to understand its role in terms of rate control in this context. We performed comparative experiments that explored the control relationship between Pab1 and eIF1 (Figs. 3D and 4D). Once again, the minimal R_1^J value of eIF1 was maintained over a wide range of Pab1 abundance values (100% to 50% of wild type abundance; Fig. 3D). In the mirror experiment, reductions in eIF1 abundance to 50% of the wild-type abundance did not affect the very low R_1^J value of Pab1 (Fig. 4D). Again, the computational model predicts (Fig. 3B and 4B) the observed general form of the experimental curves for the eIF1/Pab1 pair.

Rate control interactions across mRNA recruitment, elongation and termination

For the purpose of comparison, we extended our experimental analysis of the inter-factor rate control relationships so that the overall study would include high-flux-control factors (with high

response coefficients or R_1^J values [7]) that are involved in three of the four steps outlined in Fig. 1E: eIF4E (capped-mRNA-ribosome recruitment [17]), eEF1A (elongation [9]) and eRF1 (termination [15]). The computational model has a reduced capability to predict the interdependence relationships involving elongation (or termination) because a minimal reading frame length is used that makes the model less well suited to simulating events on the longer reading frames that are typically found on eukaryotic mRNAs. This seems to be reflected in our comparative assessment of the modelling predictions with the experimental data (Figure 9). The experimental data highlight the distinct rate control characteristics of steps outside of the scanning process (see also the flux control coefficients for the respective dual modulation experiments in the Supplementary Data section). Down-regulation of eIF4E against two reduced abundance levels of eEF1A was found to result in lessened responsiveness of translation rate in relation to eIF4E abundance (Fig. 9A), suggesting that the role of the cap-binding protein in mRNA-ribosome recruitment had become quantitatively less significant under conditions of constrained elongation. Examination of the model prediction for this relationship (Fig. 9B) reveals that this effect is captured by the modelling prediction, but that the model predicts a transition of the eIF4E R_1^J value to zero at a higher concentration of eEF1A. In the mirror experiment (Fig. 9C), the eEF1A R_1^J value dropped towards zero as the eIF4E abundance was reduced below 50%, suggesting a reciprocal interdependence of the rate control of the two factors. Here, the computational model predicted a transition of the eEF1A R_1^J value to zero at comparatively high eIF4E abundance levels (Fig. 9D).

The experimental rate control interdependence plots for eEF1A and eRF1 are markedly different. We observed no significant changes in R_1^J for eRF1 at reduced levels of eEF1A (Fig. 9E), whereas the R_1^J value for eEF1A changed minimally at lower levels of eRF1 (Fig. 9G). The computational model, in contrast, predicted transitions to a zero R_1^J value for the first titrated factor in each pair as the abundance of the second factor is reduced (Fig. 9F,H). Overall, we conclude that the experimental data reveal more complex behaviours that are readily distinguishable from the relationships that we find to be typical for the scanning-related factors. At the same time, while correctly predicting high R_1^J values for the individual factors eIF4E, eEF1A and eRF1, the computational model is less able to capture the observed interdependence of rate control for these factors.

Discussion

Molecular systems biology, the combination of computational modeling with quantitative biochemical and biophysical analysis, is an essential platform for the elucidation of principles of control in complex biomolecular systems. Indeed, characterisation of the quantitative principles of control operating in a biological system, like elucidation of structural and functional data on molecular components, is critical to a complete understanding of cell biology. In this study, we have examined the translation machinery, a highly complex system that, in one form or another, is at the heart of function and viability in all living organisms. The underpinning basis of control in such a system is not readily amenable to intuitive deduction, but here we present tools that provide valuable insight into fundamental control relationships between different steps on the protein synthesis pathway, thus enabling us to build a digital representation that will find broad application.

A computational model is only as valuable as the predictions it makes are verifiable. In this molecular systems biology approach, we have developed experimental tools that enable us to subject a highly detailed model of eukaryotic protein synthesis to validation. The observed lack of mutual influence of rate control behavior (in the near-physiological abundance range) for the two pairs of translation factors eIF1/eIF5 and eIF1/Pab1 confirms the validity of the model-based prediction that the translation machinery is configured so as to minimize the impact of scanning on flux through the protein synthesis pathway. Moreover, Pab1, which interacts with both the poly[A] tail and the 5' region of the mRNA (via the cap-binding complex), is a low R_1^J -value multifunctional factor that also manifests minimal mutual influence over the control properties of other low R_1^J – value factors. Thus, in conclusion, the dual-site analysis approach demonstrates that scanning is a low-flux-control phase that bridges two high-flux-control steps, i.e. assembly of the cap-binding complex on the 5'end of the mRNA, and polypeptide elongation. At the same time, this study confirms the validity of the model prediction that combining low-flux-control steps imposes small flux changes in the overall pathway. We have therefore identified a novel collective property of the scanning-promoting translation initiation factors that participate in this low-flux-control part of the translation pathway. This includes all of the MFC proteins (Fig. 1B), thus indicating that the MFC as a whole is a low-flux-control complex.

However, we also note that comparison of the modeling and experimental data reveals

discrepancies under conditions of more extreme inhibition. For example, the experimental rate control behaviour (Figs. 3C and 4C) observed for eIF1 and eIF5 deviates from the model predictions (Figs. 3A and 4A) at more extreme degrees of limitation of the second factor abundance. These discrepancies are evident at factor abundance levels well below the physiologically normal intracellular levels, and we suspect that they occur because more complex behaviours begin to apply under conditions that become increasingly aberrant in relation to the normal growing cell. In the modeled scenarios in which we have changed the abundance levels of two factors, everything else has remained fixed. In a living cell, in contrast, major changes in the expression of even just one gene are likely to distort the expression of other genes. Under such conditions, a model that focuses only on one subcellular machinery becomes inadequate, especially where the imposed changes result in marked growth restriction. It is for this reason that *in vivo* rate control models are most useful when used to analyse the effects of [relatively small] parameter changes that do not result in major deviations from the standard physiological state of the cell. Over time, it may become possible to create [far more comprehensive] digital representations of global cellular activities that are capable of reflecting the complex effects that arise when intracellular processes are highly distorted.

Equally remarkable are the quite distinct experimentally determined rate control relationships for the paired high-flux-control factors that operate within the other steps in the translation pathway (Fig. 9). These confirm the status of capped-mRNA-ribosome recruitment, elongation and termination as steps of strong control in the translation machinery. As the abundance of eEF1A is reduced, the rate of elongation is constrained. As a result, it is expected that the throughput [rate of translocation] of elongating ribosomes on the mRNA population is attenuated, thus increasing the proportion (and mRNA packing density) of ribosomes actively engaged in elongation (Fig. 1C,D). This, in turn, is observed to reduce the maximum attainable number of initiations per unit time, most likely by virtue of the reduced size of the intracellular pool of ribosomal subunits. This is then reflected in a suppressed requirement for eIF4E-mediated mRNA-ribosome recruitment events (Fig. 9A). In the mirror experiment, we hypothesise that slowing eIF4E-mediated mRNA-ribosome recruitment limits the requirement for eEF1A-promoted elongation cycles, possibly because there are fewer ribosomes actively elongating polypeptides on

mRNA templates (Fig. 9C). The computational model is partially capable of capturing the observed transitions in R_1^J values for these two factors.

On the other hand, the experimentally observed relationships between the activities of eEF1A and eRF1 are markedly different (Fig. 9E,G), and are likely to be affected by two factors. First, a slowing of the termination step directly influences the size of the pool of ribosomal subunits that is available for initiation by holding them up on the mRNA. Second, reductions in eRF1 abundance do not relate in a simple way to actual polypeptide terminations, because lower eRF1 activity is expected to enable, at least on some mRNAs, stop codon read-through to lead to terminations at alternative stop codons further downstream rather than to simply block termination *per se* [34]. It is difficult to characterize accurately the relative importance of the second effect, but it is likely to be less significant than that of the first point outlined above. In the case of the interdependence of rate control by eEF1A and eRF1, there are marked discrepancies between the experimental data and the model predicitions. Apart from the limitations imposed by the use of a short reading frame in the model, it is important to point out that it also does not include steps that can reflect the effect of varying eRF1 abundance on translational readthrough.

Overall, these investigations show that scanning has evolved in eukaryotes as a highly efficient process that couples ribosome recruitment to polypeptide initiation, elongation and termination on each mRNA. We conclude that there is excess capacity in the scanning-associated factors that renders the scanning process non-limiting [due to abundance values in excess of requirements], thus limiting the impact of stochastic variations in scanning machinery capacity on global protein synthesis. This suggests that the cell expends a little extra energy in producing a small excess of the scanning-related factors in order to prevent rate limitation at this non-synthetic step that couples 40S-mRNA recruitment with initiation at the start codon. Another aspect, which is beyond the scope of the present study, is that the factor requirements for scanning may change depending on the length of the 5'UTR. More specifically, it has been observed that the DEAD helicase Ded1 (and perhaps also Dbp1) exerts a particularly strong scanning-promoting role in the case of long 5'UTRs [26]. We believe that this aspect of the scanning process is worthy of further attention in future work.

This study illustrates how a molecular systems biology strategy can generate powerful

insight into the quantitative rate control characteristics of a complex cellular pathway, insight that cannot be achieved by qualitative procedures. The utilization of calibrated quantitative mass spectrometry allows comparative determination of the abundance levels across multiple components of the translation machinery, and is an approach that greatly enhances the analytical accuracy and power of rate control studies. It also highlights that the use of major disruptions of protein activity, whether caused by gene deletions or mutations or by large-scale modulation of gene expression, is likely to provide a sub-optimal basis for assessing the roles, particularly in terms of system control, of specific proteins in cellular machineries. This is because of the [often complex] collateral impact of disruptive changes on other cellular components. Minimally disruptive modulations that keep the cell close to its normal physiological state are more suitable for elucidating how a cellular machinery is controlled. As a consequence, the strategy we describe should be able to contribute to the ultimate digitization of cellular processes, a goal that must be at least partially attained if we are ever to approach an accurate [and predictive] understanding of the behavioural features that underpin the remarkable properties of living organisms. Progress in achieving this aim will of course depend upon further improvement of the computational models that are used in analysing system behaviour.

Materials and methods

Computational modelling

A computational model of translation that we developed previously [7] was the starting point for the modelling work described in this paper. The model is freely available from the BioModels database [35] with identifier BIOMD0000000457. Briefly, this is a differential equation-based model describing initiation, elongation, and termination. The model contains 156 distinct chemical species, 141 reactions, and 56 rate constants. The steady state concentrations of the various proteins were determined by mass spectrometry, while the model parameters were calibrated by fitting to 212 distinct steady states obtained by titration of individual translation factor proteins [7]. Here, we have simulated double-modulation experiments by using the parameter scan task in COPASI, where the initial concentration of each protein of a pair is set to fractions of their steady state value in the original model (from 100% down to 40%). This generates predictions for the

steady-state translation rate of 49 distinct pairs of concentrations of the two proteins (while all other proteins are kept at their steady-state concentrations). All computations were carried out using the software COPASI [36,37] version 4.24.

Strain construction

Strains used in this study were all derived from the background strain PTC41: *MATα ade2-1 ura3-1 leu2-3,112 his3-11,15 can1-100* (a derivative of W303). Promoters (P_{tetO7} with *kanMX* and P_{CuR3} with *HIS5* marker) were PCR-amplified from the vectors pCM225 [31] and TOOL-P_{CuR3} (created for this study; Fig. 7 and Supporting information section), respectively, using primers that include sequences homologous to target promoter regions to enable substitution of the region -60 to -1 upstream of each translation factor CDS with one of the regulatable promoter/5'UTR cassettes. After integration, the *HIS5* marker was removed from the P_{CuR3} promoter; it could therefore be used independently for the integration of 'top-up' constructs, which served to help adjust selected translation factor levels to the required levels [7]. Expression 'top-up' constructs were genomically integrated using either the *HIS5* marker targeted to the *can1* locus or the *BLE* (phleomycin resistance) marker targeted to the *lys2* locus. For the eEF1A strain, top-up expression was achieved by substituting the natural P_{TEF2} promoter with the P_{HYP2} promoter. A full strains table is provided in the Supporting information section.

Dual-site rate control experiments

In order to accurately determine growth rate (in YNBD-Met(-Ura) medium), protein synthesis rate (by ^{35}S-L-methionine incorporation) and relative translation factor abundance (using mass spectroscopy), a strict 3-day experimental routine was followed. Each set of cultures included two independent PTC41 control cultures and measurements involved up to 10 different test conditions. On the first day, overnight cultures (of PTC41 and of the test strain) in 10 ml of YNBD-Met(-Ura) were inoculated with single colonies from plates no more than 3 weeks old. The next morning, these cultures were diluted to OD_{600}=0.2 in 10 ml of YNBD-Met(-Ura), grown for 5 to 6 hours to reach exponential phase and then diluted to OD_{600}=0.004-0.02 in 20 ml of YNBD-Met(-Ura)

(depending on expected growth rates; the slower the growth, the higher the starting OD_{600} set by dilution), followed by overnight growth for 17 hours (to OD_{600} of approximately 1.2).

At this stage, pre-selected doxycycline and copper concentrations were established in each culture. Exploratory experiments were performed in order to identify the concentrations of these regulatory ligands that would enable us to cover the required range of translation factor abundances, and thus translation rates. 17 hours of further growth in the presence of doxycycline and copper ensured that the inhibitory effect on transcription of the targeted translation factor gene was stably reflected in steady state mRNA and encoded protein levels. On the third day, the cultures were diluted again in 20 ml of YNBD-Met(-Ura), maintaining the same doxycycline and copper concentrations, to OD_{600}=0.10-0.25. Only cultures that had similar OD_{600} values to the PTC41 reference strain were diluted and used for further experiments. To determine exponential growth rates, the optical density was monitored over the following 4.5 hours until the cultures reached OD_{600}=0.5. At this point, samples for Western blotting were collected (an equivalent of 10 ml of cells at OD_{600}=0.5), and the cultures were diluted to OD_{600}=0.1 in 10 ml of YNBD-Met(-Ura) (again, only the cultures with the same optical density as PTC41 were processed). After a further 15 minutes of growth, 100 µl of labelling mix (0.38 MBq of ^{35}S-L-methionine in 2 µg/ml methionine) was added to the each culture and samples were collected every 3 minutes (over the next 12 minutes; 5 samples in total per culture). The proteins in each sample were precipitated by TCA and the amount of radioactivity incorporated into proteins was measured using a scintillation counter [38]. In all cases there was linear accumulation of radioactivity over time, and the slope was used to calculate the relative protein synthesis rate in relation to PTC41.

Mass spectrometry

Each strain was grown in triplicate, using the same 3-day growth protocol as for the protein synthesis/growth rate measurements. For each experiment, a 20 ml yeast culture was incubated with shaking at 30°C until OD_{600}=0.5 was reached. After centrifugation and resuspension in 50 mM NH_4HCO_3, 15 ml of each culture was then transferred to a bead-beater tube and stored at -20 ˚C. Subsequently, after thawing, glass beads were added in 50 ul of 50 mM NH_4HCO_3 and the tubes were shaken in the bead beater (10 x 1 minute shaking periods, with 2 minute breaks in between).

The tubes were then pierced with a hot needle and centrifuged so that the lysate could be collected and placed into low-bind Eppendorf tubes. A 10 µl sample was taken from each tube for measurement of the lysate concentration using a NanoDrop spectrophotometer (ThermoFisher Scientific, USA). Lysates were stored at -20˚C until trypsin digestion was performed, and subsequently transferred to -80 ˚C for long-term storage. For digestion, 1.1 mg of lysate (equivalent to approximately 60 million cells) was incubated with trypsin [according to a previously described protocol [39]). Digested samples were stored at -20˚C until prepared for mass spectrometry; this preparation involved mixing 12 µl of each digest, 100 µl of a mixture of peptide standards, comprising 2.5 nM GluFib peptide (F3261, Sigma Aldrich) and ^{13}C-L-Arg/^{13}C-L-Lys-labelled, trypsin-digested Ribo3 QconCAT protein (comprising peptides corresponding to multiple translation factors, as described in reference [7]), and 88 µl of NH_4HCO_3 buffer. Mass spectrometry measurements were performed on a Thermo Scientific™ TSQ Quantiva™ Triple Quadrupole Mass Spectrometer with an UltiMate 3000 RSLCnano System (Thermo Scientific). Data analysis was performed using Skyline software [40]. The relative protein concentration was determined by dividing each abundance value by the reference value obtained for PTC41 (see Supporting information section).

References

1. Anderson PW (1972) More is different. *Science* **177**, 393-396.

2. Jackson RJ, Hellen CUT and Pestova TV (2010) The mechanism of eukaryotic translation initiation and principles of its regulation. *Nature Rev Mol Cell Biol* **11**, 113-127

3. Merrick WC and Nyborg J (2000) in *Translational control of gene expression*, eds. Sonenberg N, Hershey JWB, Mathews MB (Cold Spring Harbor Laboratory Press, Cold Spring Harbor), pp. 89–126.

4. Jackson RJ, Hellen CU and Pestova TV (2012) Termination and post-termination events in eukaryotic translation. *Adv Protein Chem Struct Biol* **86**, 45–93.

5. Duarte NC, Herrgard MJ and Palsson BO (2004) Reconstruction and validation of *Saccharomyces cerevisiae* iND750, a fully compartmentalized genome-scale metabolic model. *Genome Res* **14**, 1298-1309.

6. Spriggs KA, Bushell M and Willis AE (2010) Translational regulation of gene expression during conditions of cell stress. *Mol Cell* **40**, 228-237.

7. Firczuk H, Kannambath S, Pahle J, Claydon A, Beynon R, Duncan J, Westerhoff H, Mendes P and McCarthy JEG (2013) An *in vivo* control map for the eukaryotic mRNA translation machinery. *Mol Sys Biol* **9**, 635.

8. Lee JH, Pestova TV, Byung-Sik Shin, Chune Cao, Sang K Choi, and Dever TE (2002) Initiation factor eIF5B catalyzes second GTP-dependent step in eukaryotic translation initiation. *Proc Natl Acad Sci USA* **99**, 16689-16689

9. Taylor DR, Frank J, and Kinzy TG (eds.) (2006) Structure and function of the eukaryotic ribosome and elongation factors. Cold Spring Harbor Laboratory Press, Cold Spring Harbor, NY

10. Das S, Ghosh R and Maitra U (2001) Eukaryotic translation factor 5 functions as a GTPase-activating protein. *J Biol Chem* **276**, 6720-6726.

11. Bourgeois CF, Mortreux F and Auboeuf D (2016) The multiple functions of RNA helicases as drivers and regulators of gene expression. *Nature Rev Mol Cell Biol* **17**, 426-438.

12. Linder P and Jankowsky E (2011) From unwinding to clamping – the DEAD box RNA helicase family. *Nature Rev Mol Cell Biol* **12**, 505-516.

13. Topisirovic I, Svitkin YV, Sonenberg N and Shatkin AJ (2011) Cap and cap-binding proteins in the control of gene expression. *Wiley Interdisciplinary Rev RNA* **2**, 277-298.

14. Sokabe M, Fraser CS and Hershey JW (2012) The human translation initiation multi-factor complex promotes methionyl-tRNAi binding to the 40S ribosomal subunit. *Nucleic Acids Res* **40**, 905-913.

15. Nakamura N and Ito K (2011) tRNA mimicry in translation termination and beyond. *Wiley Interdisciplinary Rev RNA* **2**, 647-668.

16. Le Novère N, Hucka M, Huaiyu Mi, Moodie S, Schreiber F, Sorokin A, Demir E, Wegner K, Aladjem MI, Wimalaratne SM, Bergman FT, Gauges R, Ghazal P, Kawaji H, Li L, Matsuoka Y, Villéger A, Boyd SE, Calzone L, Courtot M, Dogrusoz U, Freeman TC, Funahashi A, Ghosh S,

Jouraku A, Kim S, Kolpakov F, Luna A, Sahle S, Schmidt E, Watterson S, Wu G, Goryanin I, Kell DB, Sander C, Sauro H, Snoep JL, Kohn K and Kitano H (2009) The Systems Biology Graphical Notation. *Nature Biotech* **27**, 735-741.

17. Gingras AC, Raught B and Sonenberg N (1999) eIF4 initiation factors: effectors of mRNA recruitment to ribosomes and regulators of translation. *Annu Rev Biochem* **68**, 913-963.

18. Linder P and Jankowsky E (2011) From unwinding to clamping – the DEAD box RNA helicase family. *Nat Rev Mol Cell Biol* **22**, 505-516.

19. Andreou AZ and Klostermeier D (2012) The DEAD-box helicase eIF4A. *RNA Biology* **10**, 19-32.

20. Tarun SZ, Wells SE, Deardoff JA and Sachs AB (1997) Translation initiation factor eIF4G mediates *in vitro* poly(A) tail-dependent translation. *Proc Natl Acad Sci USA* **94**, 9045-9051.

21. Otero LJ, Ashe MP and Sachs AB (1999) The yeast poly(A)-binding protein Pab1p stimulates *in vitro* poly(A)-dependent and cap-dependent translation by distinct mechanisms. *EMBO J* **18**, 3153-3163.

22. Kahvejian A, Svitkin YV, Sukarieh R, M'Boutchou MN and Sonenberg N (2005) Mammalian poly(A)-binding protein is a eukaryotic translation initiation factor, which acts via multiple mechanisms. *Genes Dev* **19**, 104–113.

23. Wolf J, Valkov E, Allen MD, Meineke B, Gordiyenko Y, McLaughlin SH, Olsen TM, Robinson CV, Bycroft M, Stewart M and Passmore LA (2014) Structural basis for Pan3 binding to Pan2 and its function in mRNA recruitment and deadenylation. *EMBO J* **33**, 1514-1526

24. Senissar M, Le Saux A, Belgareh-Touzé N, Adam C, Banroques J and Tanner NK (2014) The DEAD-box helicase Ded1 from yeast is an mRNP cap-associated protein that shuttles between the cytoplasm and nucleus. *Nucleic Acids Res* **42**, 10005-10022.

25. de la Cruz JI, Iost I, Kressler D and Linder P (1997) The p20 and Ded1 proteins have antagonistic roles in eIF4E-dependent translation in *Saccharomyces cerevisiae*. *Proc Natl Acad Sci USA* **94**, 5201-5206.

26. Berthelot K, Muldoon M, Rajkowitsch L, Hughes J and McCarthy JEG (2004) Dynamics and processivity of 40S ribosome scanning on mRNA in yeast. *Mol Microbiol* **51**, 987-1001.

27. Andersen CBF, Becker T, Blau M, Anand M, Halic M, Balar B, Mielke T, Boesen T, Pedersen J S, Spahn CMT, Kinzy TG, Andersen GR and Beckmann R (2006) Structure of eEF3 and the mechanism of transfer RNA release from the E-site. *Nature* **443**, 663–668.

28. Sonenberg N and Hinnebusch A (2009) Regulation of translation initiation in eukaryotes: mechanisms and biological targets. *Cell* **136**, 731-745.

29. Tong AH, Evangelista M, Parsons AB, Xu H, Bader GD, Pagé N, Robinson M, Raghibizadeh S, Hogue CW, Bussey H, Andrews B, Tyers M and Boone C (2001) Systematic genetic analysis with ordered arrays of yeast deletion mutants. *Science* **294**, 2364-2368.

30. Labbé S, Zhu Z and Thiele DJ (1997) Copper-specific transcriptional repression of yeast genes encoding critical components in the copper transport pathway. *J Biol Chem* **272**, 15951-15958.

31. Belli G, Garí E, Piedrafita L, Aldea M and Herrero E (1998) An activator/repressor dual system allows tight tetracycline-regulated gene expression in budding yeast. *Nucleic Acids Res* **26**, 942-947.

32. Loughran G., Sachs MS, Atkins JF and Ivanov IP (2011) Stringency of start codon selection modulates autoregulation of translation initiation factor eIF5. *Nucleic Acids Res* **40**, 2898-2906.

33. Martin-Marcos P, Cheung Y-N and Hinnebusch AG (2011) Functional elements in initiation factors 1, 1A, and 2β discriminate against poor AUG context and non-AUG start codons. *Mol Cell Biol* **31**, 4814-4831.

34. Merritt GH, Naemi WR, Mugnier P, Webb HW, Tuite MF and von der Haar T (2010) Decoding accuracy in eRF1 mutants and its correlation with pleiotropic quantitative traits in yeast. *Nucleic Acids Res* **38**, 5479-5492.

35. Chelliah V, Juty N, Ajmera I, Ali R, Dumousseau M, Glont M, Hucka M, Jalowicki G, Keating S, Knight-Schrijver V, Lloret-Villas A, Natarajan KN, Pettit JB, Rodriguez N, Schubert M, Wimalaratne SM, Zhao Y, Hermjakob H, Le Novère N, Laibe, C (2015) BioModels: ten-year anniversary. *Nucleic Acids Res* 43:D542-548. PMID:25414348.

36. Hoops S, Sahle S, Gauges R, Lee C, Pahle J, Simus N, Singhal M, Xu L, Mendes P, Kummer U (2006) COPASI — a COmplex PAthway SImulator. *Bioinformatics* **22**, 3067-3074 PMID: 17032683

37. Kent E, Hoops S and Mendes P (2012) Condor-COPASI: High-Throughput Computing for Biochemical Networks. *BMC Systems Biology* **6**, 91 PMID:22834945

38. Sangthong P, Hughes J and McCarthy JEG (2007) Distributed control for recruitment, scanning and subunit joining steps of translation initiation. *Nucleic Acids Res* **35***,* 3573-3580.

39. Brownridge PJ, Harman VM, Simpson DM and Beynon RJ (2012) Absolute multiplexed protein quantification using QconCAT technology. *Methods Mol Biol* **893**, 267–293.

40. MacLean B, Tomazela DM, Shulman N, Chambers M, Finney GL, Frewen B, Kern R, Tabb DL, Liebler DC and MacCoss MJ (2010) Skyline: an open source document editor for creating and analyzing targeted proteomics experiments. *Bioinformatics* **26**, 966–968.

Figure Legends

Fig. 1. Molecular interactions and flows in eukaryotic translation. (A) Partial Petri net representation of translation scanning and initiation, in which the pathway is depicted as a series of bimolecular reactions/interactions. The scheme features the preformed multi-factor complex (MFC) and cap-binding complex bound to 5'-capped mRNA (m^7G-mRNA.eIF4F.Pab1), whose component interactions are illustrated in panel B. Scanning is depicted as a fast step that transfers each ribosomal pre-initiation complex (48S.m^7G) from the 5'cap to the site of a start codon (48S.AUG) (panels A,C). Ded1 is thought to be a low-flux-control factor that has a more readily detectable influence on scanning efficiency along longer [structured] 5'UTRs [7]. Under normal conditions, the elongation process is efficient, thus leaving sizeable gaps between elongating 80S complexes, while termination releases the separate ribosomal subunits back into the intracellular ribosome pool where they are again available for further initiation events (panel C). Attenuation of the rate of elongation, for example caused by suppression of the activity of an elongation factor such as eEF1A, is expected to cause bunching up of the elongating 80S ribosomal complexes (panel D), thus retaining a greater proportion of the intracellular pool of ribosomal subunits associated with mRNP. Each pair of factors investigated in this study was selected from the set of translation factors indicated in panel E. These factors are respectively engaged in four steps: mRNA/ribosome recruitment (eIF4E), scanning (eIF1, eIF5), elongation (eEF1A) and termination (eRF1).

Fig. 2. SBGN maps of the initiation (A) and elongation/termination (B) steps as represented in the computational model.

Fig. 3. Predicted control characteristics for scanning factor pairs. The computational model predicts the outcomes of dual-site regulatory regulation of pairs of translation factors: eIF1/eIF5 (panel A) and eIF1/Pab1 (panel B). For each pair, the expression of one translation factor gene is progressively suppressed against a background of different attenuated abundance levels of the second factor. A plateau of insensitivity is predicted in the near-physiological region of factor abundance. In other words, as the abundance of the primary factor in each pair (for example, eIF5 in panel A and eIF1 in panel B) is reduced progressively from the wild-type abundance [100%],

there is a zone in which the global translation rate remains unchanged. The curves manifesting this plateau-type behaviour are coloured in blue. In panel A, the plateau is no longer evident in those curves generated at lower (below 80%) abundance values of the secondary factor (coloured in red). The corresponding experimental dual-site control data are presented in panels C (eIF5/eIF1) and D (eIF1/Pab1). Expression of each of the genes encoding the respective translation factors was progressively and independently down-regulated using genomic P_{CuR3} and P_{tetO7} regulatory promoter constructs. The abundance of each factor was determined using calibrated mass spectrometry (Fig. 8). In each case, the abundance of the 'primary' factor in the pair is plotted as a percentage of the wild-type abundance on the x-axis, while the three set levels of the secondary factor in each pair are given as abundance percentage values in the highlighted boxes within the plot areas.

Fig. 4 Mirror rate control plots to those shown in Fig. 3. The model output plot for the influence of variations in eIF1 abundance on global translation rate at different abundance levels of eIF5 (A) is compared to the equivalent experimental data (C). Similarly, the model (B) and experimental (D) plots are compared for the factor pair eIF1/Pab1.

Fig. 5 Dual-site rate control plots generated by the computational model for translation initiation factors. Predicted relationships are shown for the translation factor pairs eIF3/eIF1 (A,B) and eIF1A/eIF1 (C,D).

Fig. 6. Regulatory promoters used for dual-site modulation of the translation machinery. (A) The Mac1 transcription factor activates the promoter by binding to the copper regulatory element [CuRE], but its binding affinity is reduced in the presence of copper. The synthetic P_{CuR3} construct (A) was selected from a set of P_{CTR1} derivatives (panels B,C) in which we had inserted additional copies of the copper regulatory element (CuRE). The firefly luciferase (*LUC*) reporter gene was used to characterize the regulatory behavior of the reporters. The repressibility of the three synthetic P_{CuR} promoters (B) was similar, but overall transcriptional activity was boosted by adding additional CuREs (C). Panels B and C share the same colour coding for the respective constructs;

in addition, the green line in panel B records the activity generated by *LUC* transcribed from P_{CuR3} in the absence of added copper. P_{CuR3} was used in combination with the *tetO7* regulatory promoter (containing seven copies of the *tetO* box, which are bound by the doxycycline-repressible *tetR*-VP16 (tTA) hybrid transactivator [31]; panel D), allowing us to simultaneously (but independently) down-regulate the expression of a pair of translation factors in each experiment.

Fig. 7. Repression behaviour of the synthetic P_{CuR3} promoter. (A) Map of the plasmid (TOOL-P_{CuR3}) bearing the synthetic P_{CuR3} promoter. (B) Progressive suppression of expression of the firefly *LUC* reporter transcribed from the P_{CuR3} promoter. The addition of copper sulphate to a final concentration of 10μM results in maximal suppression. (C) The presence of 10μM copper sulphate has no effect on growth.

Fig. 8. Mass spectrometric analysis of translation factor abundance values. Typical results of quantitative mass spectrometry (presented as heat maps) are shown for experimental dual rate-control experiments involving modulation of eIF1/eIF5 (A,B), eIF1/Pab1 (C,D), eIF4E/eEF1A (E,F) and eEF1A/eRF1 (G,H). The heat maps show the abundance values for nineteen translation factors in response to the presence of different concentrations of the regulatory ligands Cu^{+} and doxycycline. Each value represented in the heat maps is derived from at least three biological repeats. The relationship of the colour scale to the relative protein abundance is indicated at the bottom.

Fig. 9. Dual-site analysis targeted to high R_1^J translation factors. Expression of each of the genes encoding the respective translation factors was progressively and independently down-regulated using genomic P_{CuR3} and P_{tetO7} regulatory promoter constructs. The abundance of each factor was determined using calibrated mass spectrometry (Fig. 8). In each case, the abundance of the 'primary' factor in the pair is plotted as a percentage of the wild-type abundance on the x-axis, while the three set levels of the secondary factor in each pair are given as abundance percentage values in the highlighted boxes within the plot areas. Each experimental dual-site rate control plot is paired with the equivalent computational model plot: eIF4E/eEF1A (A,B and C,D); eRF1/eEF1A

(E,F and G,H).

Acknowledgements

We thank Alex Jones and Cleidane Zampronio [Warwick Proteomics Platform] for help with mass spectrometry. Funding was provided by the Biotechnology & Biological Sciences Research Council UK [BB/1008349/1 and BB/1020535/1 to JEGM] and the NIH/NIGMS USA [GM080219 to PM].

Author contributions

This study was designed by JEGM and PM. Experiments were performed by HF and JT; computational modeling was performed by PM. The manuscript was written by JEGM.

Conflicts of Interest

The authors have no conflicts of interest.

Supporting information

Additional supporting information may be found online in the Supporting Information section at the end of the article.

Description of procedure to estimate protein abundance values.

Table of *S.cerevisiae* strains including expression top-up plasmids.

Complete nucleotide sequence of plasmid carrying the synthetic regulatable P_{CuR3} promoter.

Estimated R_1^J values derived from the experimental dual-site rate control data.

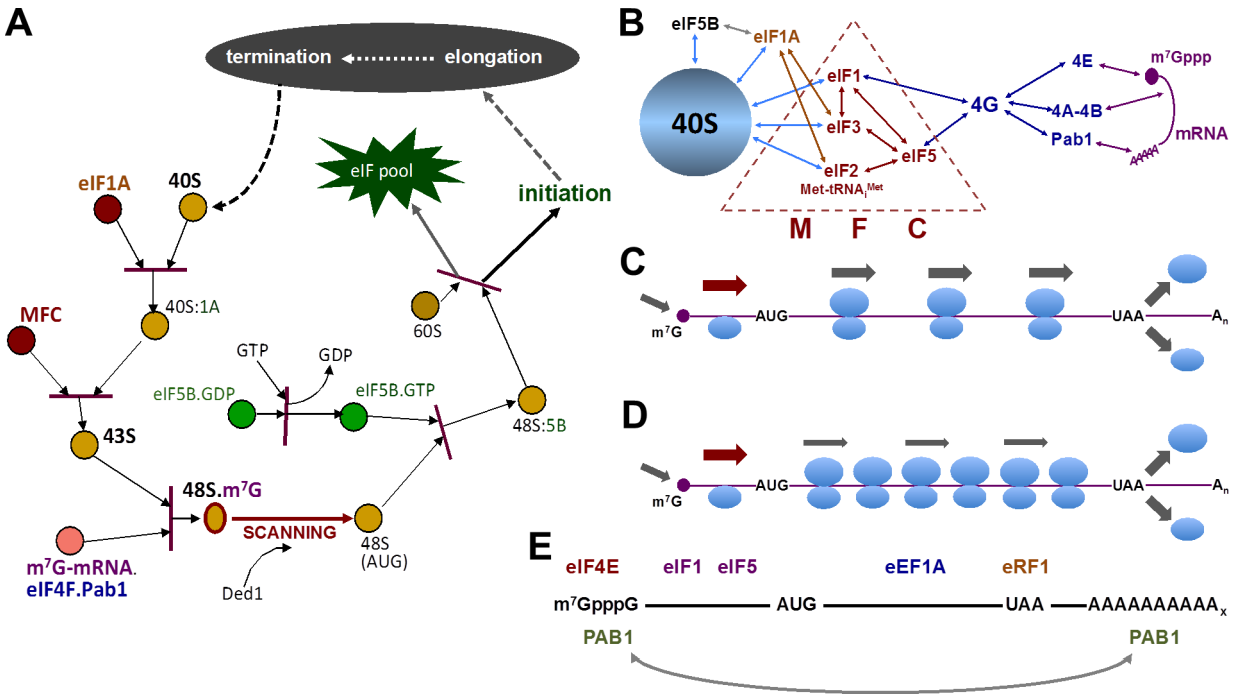
A
termination
elongation
eIF pool
initiation
eIF1A
40S
40S:1A
MFC
60S
GTP
GDP
eIF5B.GDP
eIF5B.GTP
48S:5B
43S
48S.m7G
SCANNING
48S
(AUG)
m7G-mRNA.
eIF4F.Pab1
Ded1
B
eIF5B
eIF1A
40S
eIF1
eIF3
eIF2
Met-tRNAiMet
eIF5
4G
4E
m7Gppp
4A-4B
Pab1
mRNA
M F C
C
m7G
AUG
UAA
An
D
m7G
AUG
UAA
An
E
eIF4E
eIF1
eIF5
eEF1A
eRF1
m7GpppG
AUG
UAA
AAAAAAAAAx
PAB1
PAB1

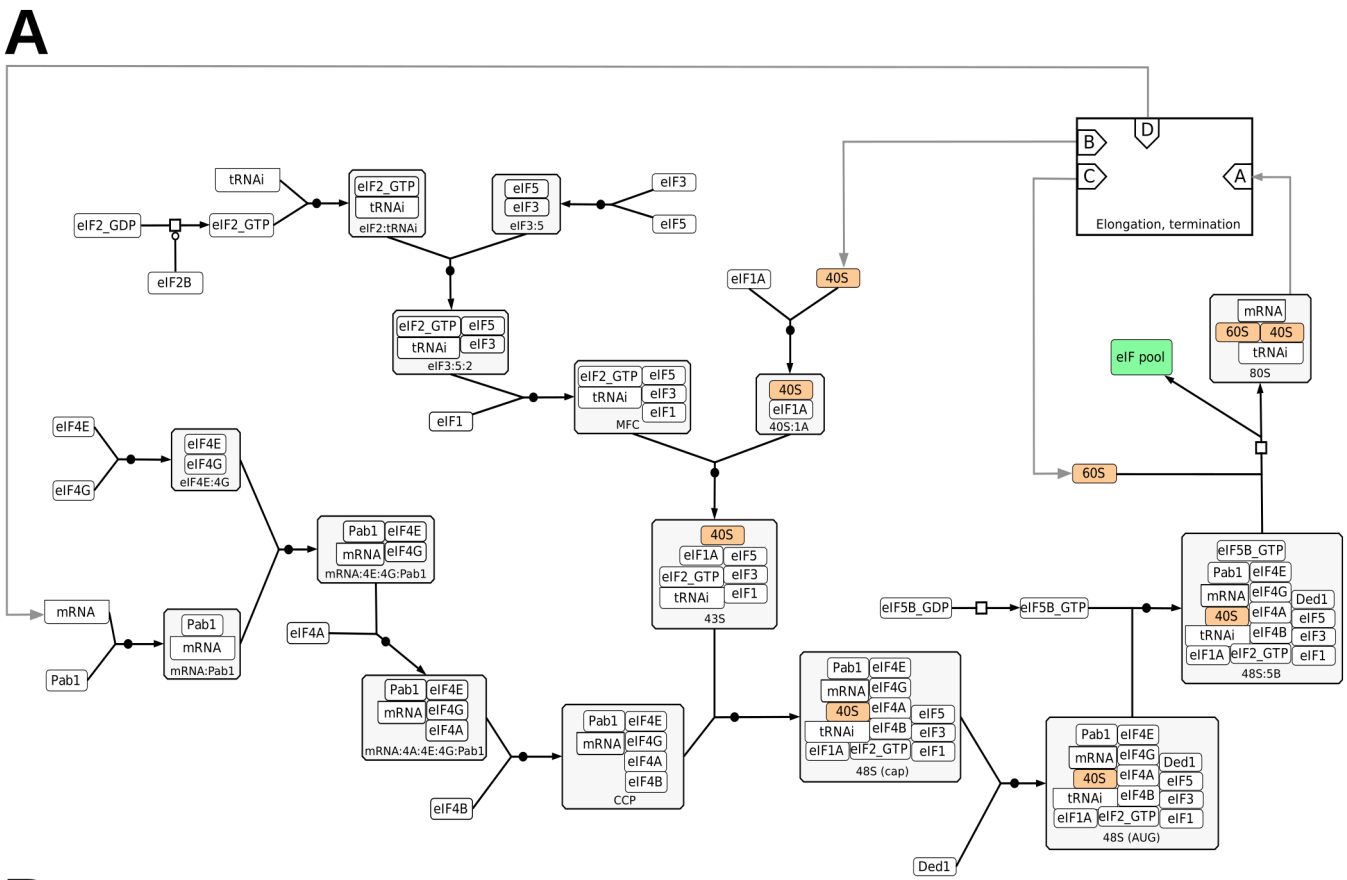
A
tRNAi
eIF2_GTP
tRNAi
eIF2:tRNAi
eIF2_GDP
eIF2_GTP
eIF2B
eIF5
eIF3
eIF3:5
eIF3
eIF5
eIF2_GTP
tRNAi
eIF5
eIF3
eIF3:5:2
eIF1
eIF2_GTP
eIF5
tRNAi
eIF3
eIF1
MFC
eIF1A
40S
40S
eIF1A
40S:1A
B
D
C
A
Elongation, termination
mRNA
60S
40S
tRNAi
80S
eIF pool
60S
eIF4E
eIF4G
eIF4E:4G
Pab1
eIF4E
mRNA
eIF4G
mRNA:4E:4G:Pab1
40S
eIF1A
eIF5
eIF2_GTP
eIF3
tRNAi
eIF1
43S
eIF5B_GDP
eIF5B_GTP
eIF5B_GTP
Pab1
eIF4E
mRNA
eIF4G
Ded1
40S
eIF4A
eIF5
tRNAi
eIF4B
eIF3
eIF1A
eIF2_GTP
eIF1
48S:5B
mRNA
Pab1
Pab1
mRNA
mRNA:Pab1
eIF4A
Pab1
eIF4E
mRNA
eIF4G
eIF4A
mRNA:4A:4E:4G:Pab1
eIF4B
Pab1
eIF4E
mRNA
eIF4G
eIF4A
eIF4B
CCP
Pab1
eIF4E
mRNA
eIF4G
40S
eIF4A
eIF5
tRNAi
eIF4B
eIF3
eIF1A
eIF2_GTP
eIF1
48S (cap)
Pab1
eIF4E
mRNA
eIF4G
Ded1
40S
eIF4A
eIF5
tRNAi
eIF4B
eIF3
eIF1A
eIF2_GTP
eIF1
48S (AUG)
Ded1
B
eEF1A_GDP
eEF1B
eEF1A_GTP
tRNA
eEF1A_GTP
aa_tRNA
aatRNA:eEF1A
aa_tRNA
60S
40S
mRNA
80S:aatRNA
eEF1A_GTP
aa_tRNA
60S
40S
mRNA
80S:aatRNA:eEF1A
eEF2_GTP
eEF2_GTP
aa_tRNA
60S
40S
mRNA
80S:aatRNA:eEF2
eEF2_GDP
60S
40S
mRNA
80S
eEF3_GDP
eEF3_GTP
tRNA
60S
40S
mRNA
80S:tRNA
eEF3_GTP
tRNA
60S
40S
mRNA
80S:tRNA:eEF3
eRF3_GTP
eRF3_GTP
eRF1
eRF1:RF3
eRF1
eRF3_GDP
eRF3_GTP
eRF1
60S
40S
mRNA
80S:eRF1:RF3
40S
60S
mRNA
B
C
D
A
Initiation

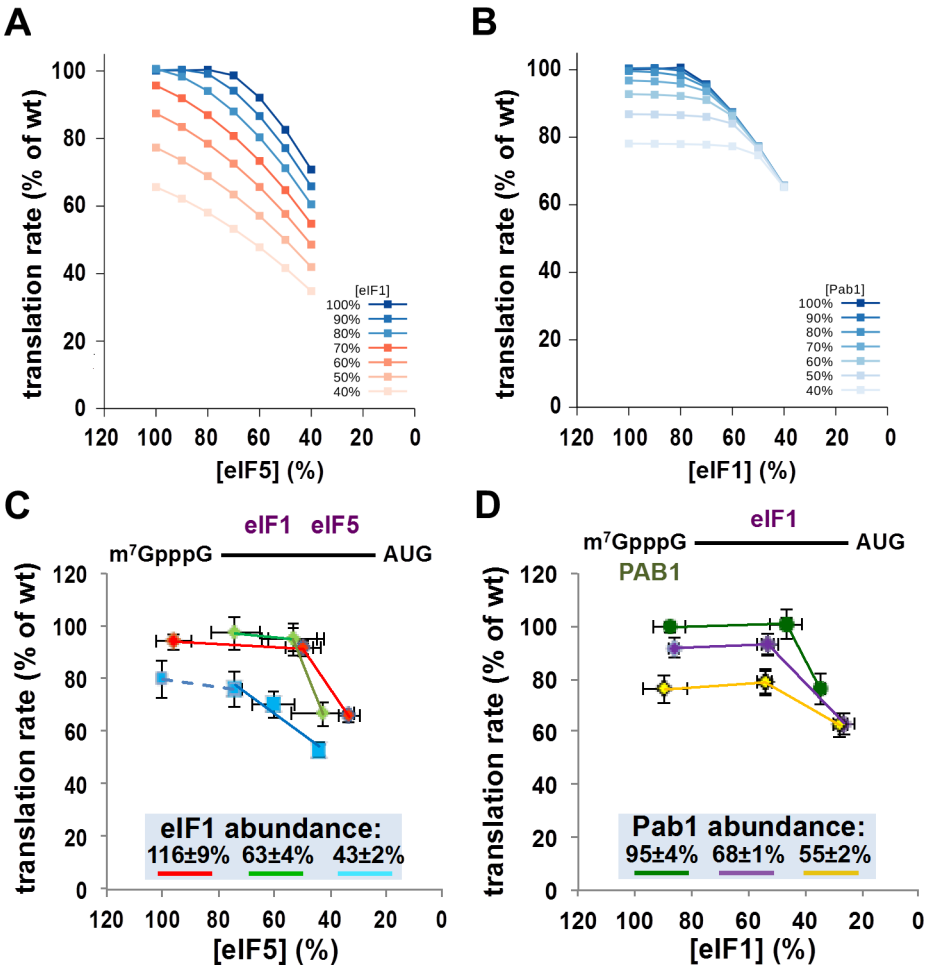
A
translation rate (% of wt)
[eIF5] (%)
[eIF1]
100%
90%
80%
70%
60%
50%
40%
B
translation rate (% of wt)
[eIF1] (%)
[Pab1]
100%
90%
80%
70%
60%
50%
40%
C
eIF1 eIF5
m7GpppG AUG
translation rate (% of wt)
[eIF5] (%)
eIF1 abundance:
116±9% 63±4% 43±2%
D
eIF1
m7GpppG AUG
PAB1
translation rate (% of wt)
[eIF1] (%)
Pab1 abundance:
95±4% 68±1% 55±2%

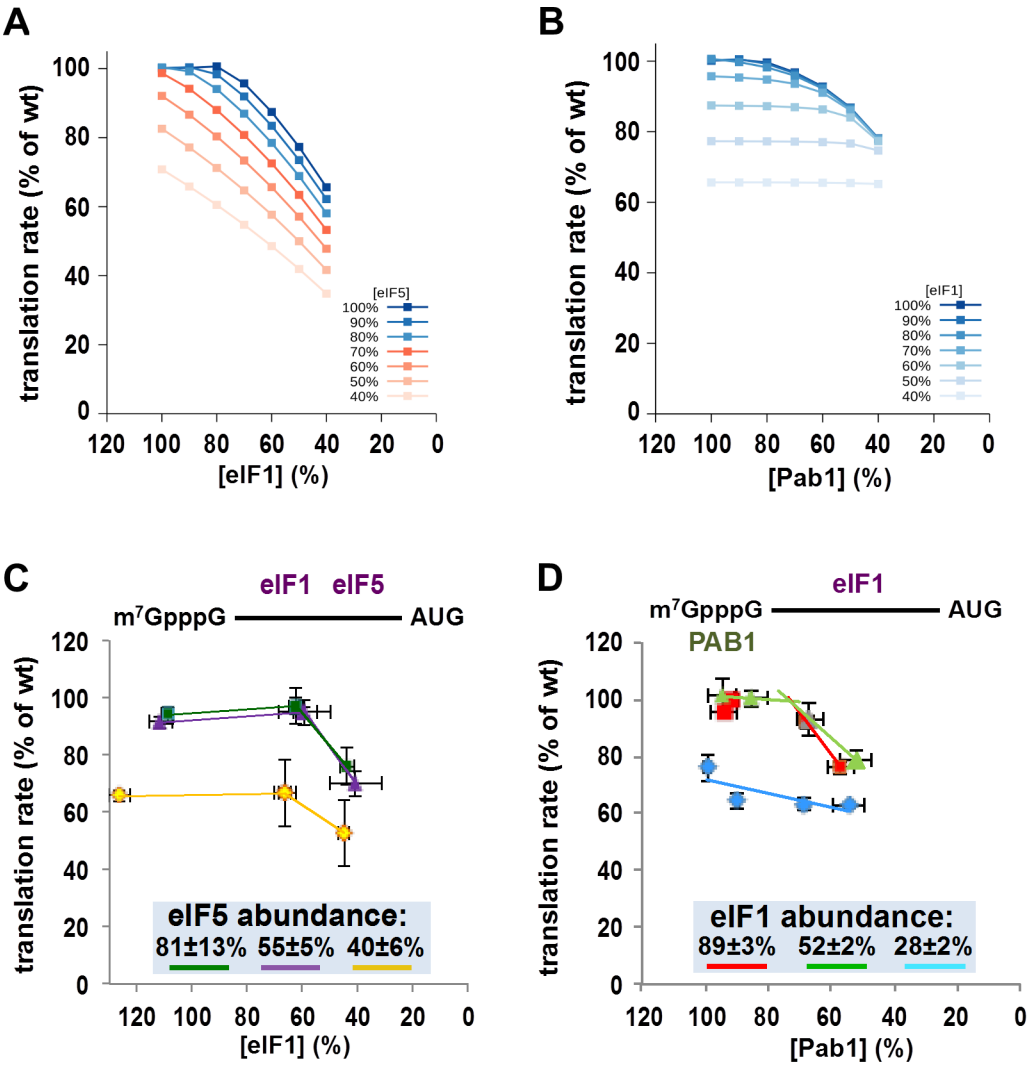
A
translation rate (% of wt)
100
80
60
40
20
0
120 100 80 60 40 20 0
[eIF1] (%)
[eIF5]
100%
90%
80%
70%
60%
50%
40%
B
translation rate (% of wt)
[Pab1] (%)
[eIF1]
C
eIF1 eIF5
m7GpppG
AUG
translation rate (% of wt)
eIF5 abundance:
81±13% 55±5% 40±6%
[eIF1] (%)
D
eIF1
m7GpppG
AUG
PAB1
translation rate (% of wt)
eIF1 abundance:
89±3% 52±2% 28±2%
[Pab1] (%)

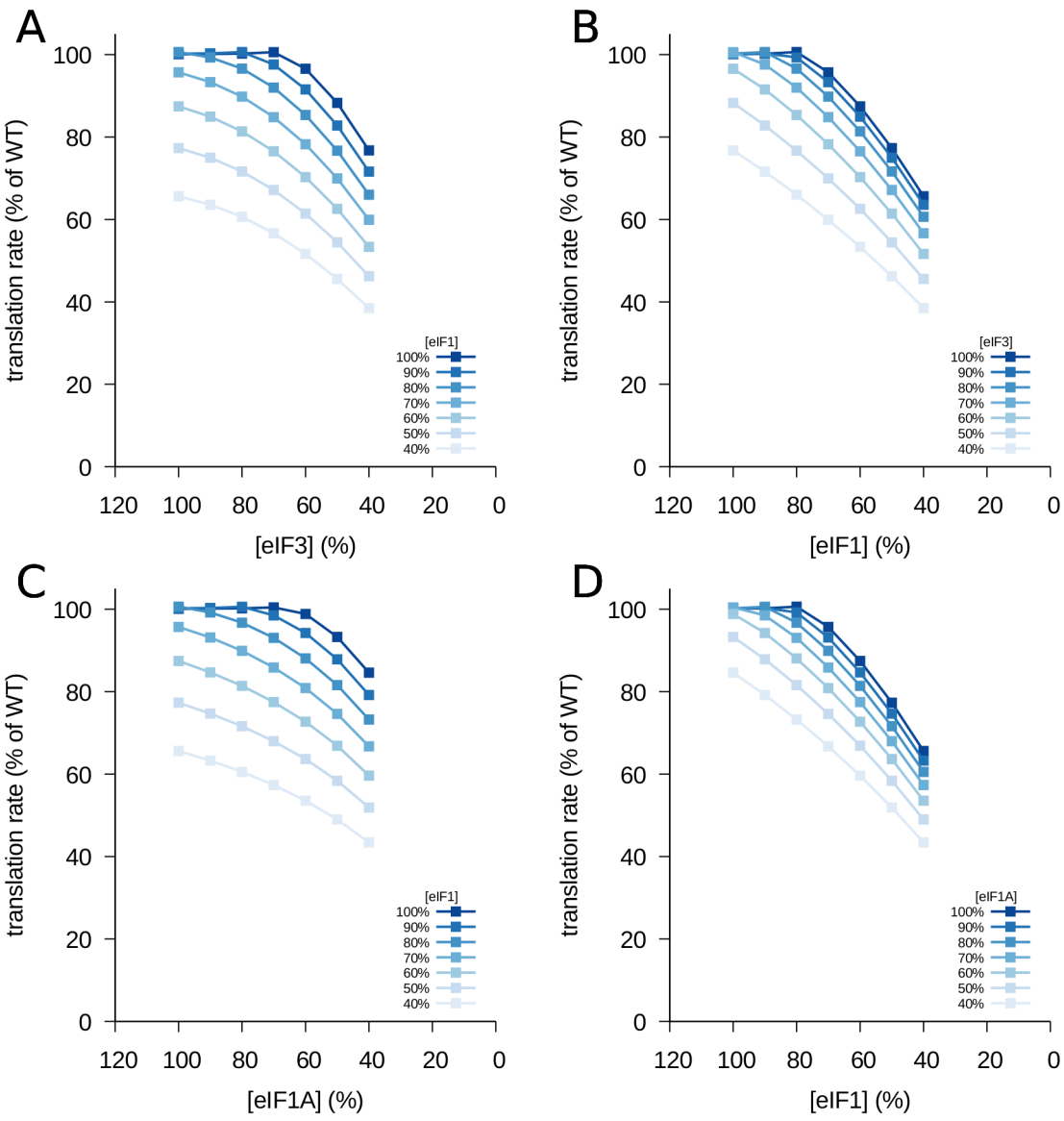
A
translation rate (% of WT)
100
80
60
40
20
0
120
100
80
60
40
20
0
[eIF3] (%)
[eIF1]
100%
90%
80%
70%
60%
50%
40%
B
translation rate (% of WT)
[eIF1] (%)
[eIF3]
C
translation rate (% of WT)
[eIF1A] (%)
[eIF1]
D
translation rate (% of WT)
[eIF1] (%)
[eIF1A]

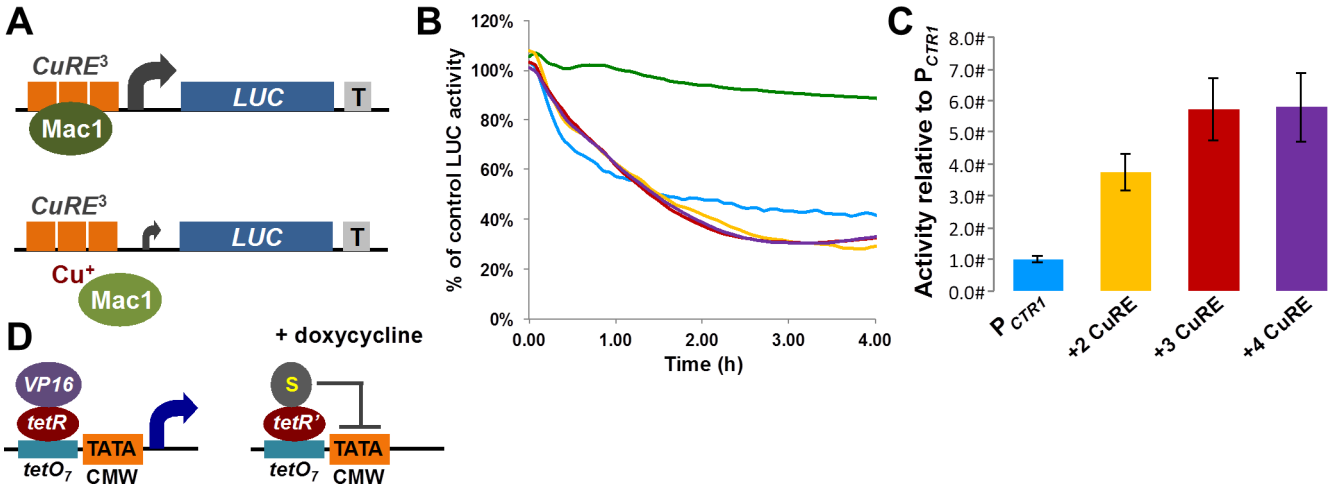
A
CuRE3
LUC
T
Mac1
CuRE3
LUC
T
Cu+
Mac1
B
% of control LUC activity
120%
100%
80%
60%
40%
20%
0%
0.00
1.00
2.00
3.00
4.00
Time (h)
C
Activity relative to P CTR1
8.0#
7.0#
6.0#
5.0#
4.0#
3.0#
2.0#
1.0#
0.0#
P CTR1
+2 CuRE
+3 CuRE
+4 CuRE
D
+ doxycycline
VP16
tetR
TATA
tetO7
CMW
S
tetR'
TATA
tetO7
CMW

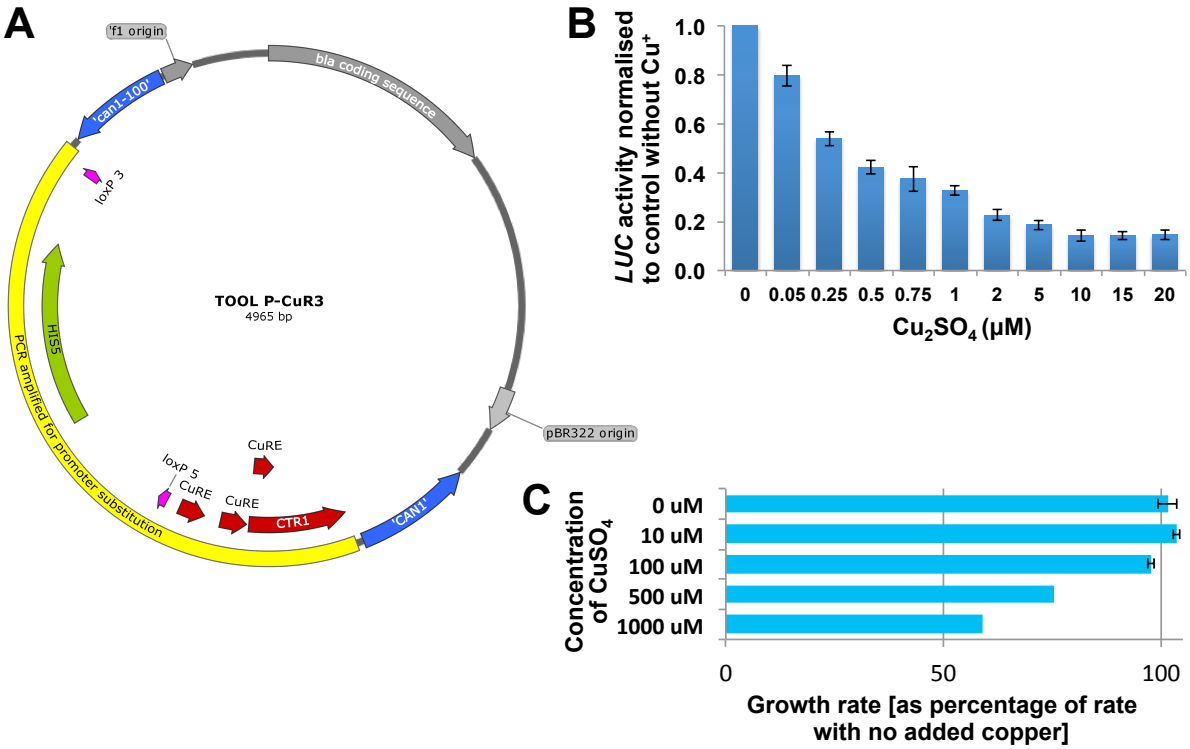
A
'f1 origin
bla coding sequence
'can1-100'
loxP 3
TOOL P-CuR3
4965 bp
HIS5
PCR amplified for promoter substitution
pBR322 origin
CuRE
loxP 5
CuRE
CuRE
CTR1
'CAN1'
B
LUC activity normalised to control without Cu+
1.0
0.8
0.6
0.4
0.2
0.0
0
0.05
0.25
0.5
0.75
1
2
5
10
15
20
Cu2SO4 (µM)
C
Concentration of CuSO4
0 uM
10 uM
100 uM
500 uM
1000 uM
0
50
100
Growth rate [as percentage of rate with no added copper]

Figure 7

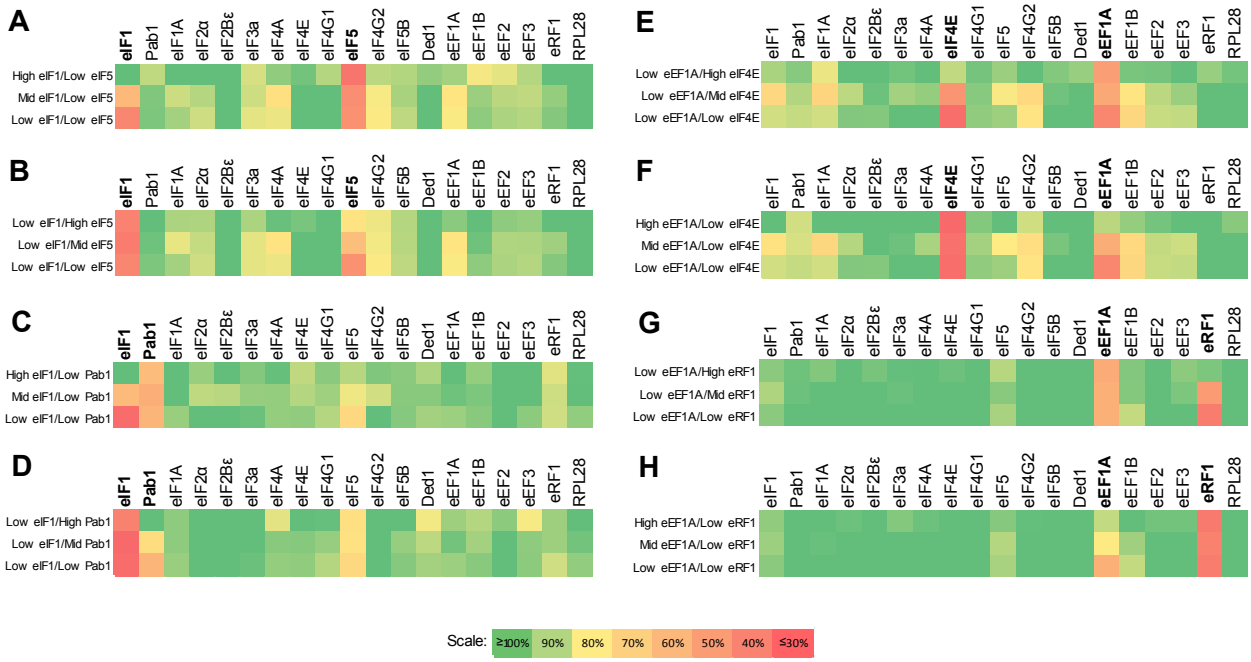
A
eIF1 Pab1 eIF1A eIF2α eIF2Bε eIF3a eIF4A eIF4E eIF4G1 eIF5 eIF4G2 eIF5B Ded1 eEF1A eEF1B eEF2 eEF3 eRF1 RPL28
High eIF1/Low eIF5
Mid eIF1/Low eIF5
Low eIF1/Low eIF5
B
eIF1 Pab1 eIF1A eIF2α eIF2Bε eIF3a eIF4A eIF4E eIF4G1 eIF5 eIF4G2 eIF5B Ded1 eEF1A eEF1B eEF2 eEF3 eRF1 RPL28
Low eIF1/High eIF5
Low eIF1/Mid eIF5
Low eIF1/Low eIF5
C
eIF1 Pab1 eIF1A eIF2α eIF2Bε eIF3a eIF4A eIF4E eIF4G1 eIF5 eIF4G2 eIF5B Ded1 eEF1A eEF1B eEF2 eEF3 eRF1 RPL28
High eIF1/Low Pab1
Mid eIF1/Low Pab1
Low eIF1/Low Pab1
D
eIF1 Pab1 eIF1A eIF2α eIF2Bε eIF3a eIF4A eIF4E eIF4G1 eIF5 eIF4G2 eIF5B Ded1 eEF1A eEF1B eEF2 eEF3 eRF1 RPL28
Low eIF1/High Pab1
Low eIF1/Mid Pab1
Low eIF1/Low Pab1
E
eIF1 Pab1 eIF1A eIF2α eIF2Bε eIF3a eIF4A eIF4E eIF4G1 eIF5 eIF4G2 eIF5B Ded1 eEF1A eEF1B eEF2 eEF3 eRF1 RPL28
Low eEF1A/High eIF4E
Low eEF1A/Mid eIF4E
Low eEF1A/Low eIF4E
F
eIF1 Pab1 eIF1A eIF2α eIF2Bε eIF3a eIF4A eIF4E eIF4G1 eIF5 eIF4G2 eIF5B Ded1 eEF1A eEF1B eEF2 eEF3 eRF1 RPL28
High eEF1A/Low eIF4E
Mid eEF1A/Low eIF4E
Low eEF1A/Low eIF4E
G
eIF1 Pab1 eIF1A eIF2α eIF2Bε eIF3a eIF4A eIF4E eIF4G1 eIF5 eIF4G2 eIF5B Ded1 eEF1A eEF1B eEF2 eEF3 eRF1 RPL28
Low eEF1A/High eRF1
Low eEF1A/Mid eRF1
Low eEF1A/Low eRF1
H
eIF1 Pab1 eIF1A eIF2α eIF2Bε eIF3a eIF4A eIF4E eIF4G1 eIF5 eIF4G2 eIF5B Ded1 eEF1A eEF1B eEF2 eEF3 eRF1 RPL28
High eEF1A/Low eRF1
Mid eEF1A/Low eRF1
Low eEF1A/Low eRF1
Scale: ≥100% 90% 80% 70% 60% 50% 40% ≤30%

Figure 8

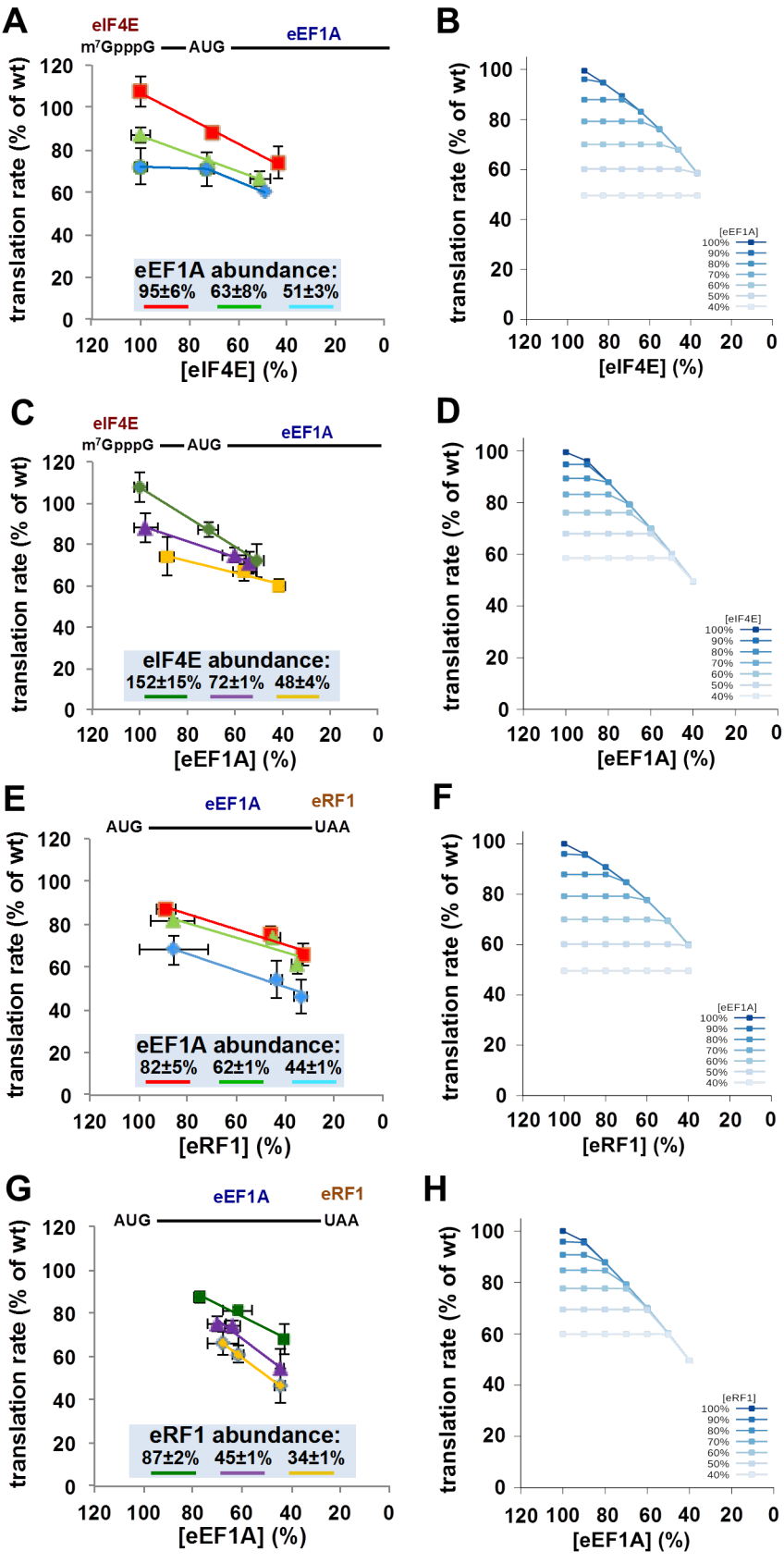
A
eIF4E
m7GpppG
AUG
eEF1A
translation rate (% of wt)
eEF1A abundance:
95±6% 63±8% 51±3%
[eIF4E] (%)
B
translation rate (% of wt)
[eEF1A]
100%
90%
80%
70%
60%
50%
40%
[eIF4E] (%)
C
eIF4E
m7GpppG
AUG
eEF1A
translation rate (% of wt)
eIF4E abundance:
152±15% 72±1% 48±4%
[eEF1A] (%)
D
translation rate (% of wt)
[eIF4E]
100%
90%
80%
70%
60%
50%
40%
[eEF1A] (%)
E
eEF1A
eRF1
AUG
UAA
translation rate (% of wt)
eEF1A abundance:
82±5% 62±1% 44±1%
[eRF1] (%)
F
translation rate (% of wt)
[eEF1A]
100%
90%
80%
70%
60%
50%
40%
[eRF1] (%)
G
eEF1A
eRF1
AUG
UAA
translation rate (% of wt)
eRF1 abundance:
87±2% 45±1% 34±1%
[eEF1A] (%)
H
translation rate (% of wt)
[eRF1]
100%
90%
80%
70%
60%
50%
40%
[eEF1A] (%)

Supporting Information

Using MS data to estimate protein abundance values

Three biological repeats were collected for each test condition. Given that there were 9 conditions for each of the four translation factor pairs, this yielded 108 samples to be analyzed using mass spectrometry. In addition, we performed 12 biological repeats of the wild-type PTC41 strain, and these samples were evenly spread between the other experimental runs. After all of the data had been collected, the results were imported into Skyline software for initial analysis.

All of the transition peaks were viewed, and the peak positions were manually corrected if the automated peak assignment was clearly misaligned. If there was no obvious solution to misaligned peaks the transitions were marked as unreliable and removed from the analysis. In this way, the total number of transitions used in this analysis was reduced from 959 to 527. The data of signal intensities of all the transitions was then exported for further analysis in Microsoft Office Excel.

The following calculations were performed for each sample:

1. The peptide signal intensity was calculated as a sum of signals from all of the transitions measured for this peptide.
2. The protein signal intensity was then calculated as a sum of signals from all of the peptides measured for a given protein.
3. The loading control intensity was calculated as a geometric mean of signals for: unlabelled GluFib peptide and labelled GluFib and Fib peptides from the Ribo3 QconCAT protein*.
4. The loading-corrected protein signal was calculated by dividing the protein signal intensity (p2) by the intensity of the loading control (p3), thus correcting the protein signal for the differences in loading.
5. The weighted calibrator signal intensity was calculated as the geometric mean of signal of the Rps5, Rpl28 and Act1 proteins.
6. The calibrated protein signal was calculated by dividing the loading-corrected protein signal (p4) by the weighted calibrator signal intensity (p5).
7. If there was a labelled reference peptide present for a given protein – it was treated in the same way as other signals, subject to calculation of the heavy to light ratio.
8. The average was calculated for the data from the biological repeats of the same condition.
9. The relative protein concentration was calculated by dividing the average value obtained for each protein by the average value obtained for the PTC41 reference strain.

* Firczuk,H., Kannambath,S., Pahle,J., Claydon,A., Beynon,R., Duncan,J., Westerhoff,H., Mendes,P. and McCarthy,J.E.G. (2013) An *in vivo* control map for the eukaryotic mRNA translation machinery. *Mol. Sys. Biol.,* **9**, 635.

TOOL-P$_{CuR3}$

Complete nucleotide sequence of plasmid shown in Supplementary Figure S2, with synthetic P$_{CuR3}$ sequence highlighted in red.

TTGGGTGCACGAGTGGGTTACATCGAACTGGATCTCAACAGCGGTAAGATCCTTGAGAGTTTTCGCCCCGAA
GAACGTTTTCCAATGATGAGCACTTTTAAAGTTCTGCTATGTGGCGCGGTATTATCCCGTATTGACGCCGGG
CAAGAGCAACTCGGTCGCCGCATACACTATTCTCAGAATGACTTGGTTGAGTACTCACCAGTCACAGAAAAG
CATCTTACGGATGGCATGACAGTAAGAGAATTATGCAGTGCTGCCATAACCATGAGTGATAACACTGCGGCC
AACTTACTTCTGACAACGATCGGAGGACCGAAGGAGCTAACCGCTTTTTTGCACAACATGGGGGATCATGTA
ACTCGCCTTGATCGTTGGGAACCGGAGCTGAATGAAGCCATACCAAACGACGAGCGTGACACCACGATGCCT
GCAGCAATGGCAACAACGTTGCGCAAACTATTAACTGGCGAACTACTTACTCTAGCTTCCCGGCAACAATTA
ATAGACTGGATGGAGGCGGATAAAGTTGCAGGACCACTTCTGCGCTCGGCCCTTCCGGCTGGCTGGTTTATT
GCTGATAAATCTGGAGCCGGTGAGCGTGGGTCTCGCGGTATCATTGCAGCACTGGGGCCAGATGGTAAGCCC
TCCCGTATCGTAGTTATCTACACGACGGGGAGTCAGGCAACTATGGATGAACGAAATAGACAGATCGCTGAG
ATAGGTGCCTCACTGATTAAGCATTGGTAACTGTCAGACCAAGTTTACTCATATATACTTTAGATTGATTTA
AAACTTCATTTTTAATTTAAAAGGATCTAGGTGAAGATCCTTTTTGATAATCTCATGACCAAAATCCCTTAA
CGTGAGTTTTCGTTCCACTGAGCGTCAGACCCCGTAGAAAAGATCAAAGGATCTTCTTGAGATCCTTTTTTT
CTGCGCGTAATCTGCTGCTTGCAAACAAAAAAACCACCGCTACCAGCGGTGGTTTGTTTGCCGGATCAAGAG
CTACCAACTCTTTTTCCGAAGGTAACTGGCTTCAGCAGAGCGCAGATACCAAATACTGTCCTTCTAGTGTAG
CCGTAGTTAGGCCACCACTTCAAGAACTCTGTAGCACCGCCTACATACCTCGCTCTGCTAATCCTGTTACCA
GTGGCTGCTGCCAGTGGCGATAAGTCGTGTCTTACCGGGTTGGACTCAAGACGATAGTTACCGGATAAGGCG
CAGCGGTCGGGCTGAACGGGGGGTTCGTGCACACAGCCCAGCTTGGAGCGAACGACCTACACCGAACTGAGA
TACCTACAGCGTGAGCTATGAGAAAGCGCCACGCTTCCCGAAGGGAGAAAGGCGGACAGGTATCCGGTAAGC
GGCAGGGTCGGAACAGGAGAGCGCACGAGGGAGCTTCCAGGGGGAAACGCCTGGTATCTTTATAGTCCTGTC
GGGTTTCGCCACCTCTGACTTGAGCGTCGATTTTTGTGATGCTCGTCAGGGGGGCGGAGCCTATGGAAAAAC
GCCAGCAACGCGGCCTTTTTACGGTTCCTGGCCTTTTGCTGGCCTTTTGCTCACATGTTCTTTCCTGCGTTA
TCCCCTGATTCTGTGGATAACCGTATTACCGCCTTTGAGTGAGCTGATACCGCTCGCCGCAGCCGAACGACC
GAGCGCAGCGAGTCAGTGAGCGAGGAAGCGGAAGAGCGCCTGATGCGGTATTTTCTCCTTACGCATCTGTGC
GGTATTTCACACCGCATATATGGTGCACTCTCAGTACAATCTGCTCTGATGCCGCATAGTTAAGCCAGTATA
CGACGTCAAGCCAAAGCGCCAAATGCAGCAGTAACGAAAACTGCAATGTATGGAACACCACCTTTGGTGGTC
CTTGACAGGAATTTAGGAGCCAACTTGTTCTTTGATAGACCAAATAAAATACGGGAACCAACGTAAATATTT
GAATTTGCGGCAGAAATAATGGTTGTTAAGATAACAGCGTTGAAGATATGTGGCAAAACCTTTGTACCAGAG
TTCTCAATAGCAATAATAAAGGGAGAAGTAGAAACGTAGGAAGTAGATTGTGTTAGTTTAGGGTCATTGTAT
GGAACTAAAAGTCCAATGAATAATAGAGAGCCAATGTAGAAGGTTAAGATACGGAAAACAACTTTTTTGATG
GCTCTTGGAACGGATTTTCTGAGGCCTTGCAAACTAGTGGCGCCATTTTGAATGTCAAATATAATACACTTT
TTTTTATTTTCTATTCGATTCTTCCAACAAATGTAATTTGAGTCGCCGCCGAACTATTACTCCACCTGTTTA
AGTTTGTGCTTAAAAGTTTTGTTATGCAAATAAAGCTATGGAGTAGTTGTTTATTAAGAGCACACTGCGTAT
CTGTTTTACTAATGTGAACTAATCATAAGAGGAATAAAACATACAAGACCCTCTCGAGATGACAATACAACA
TTTTTTATGTTGCATTTTGTAGCCCGAATCTTGAAAAGTGCTCTTTTCAGGATCGTGCCATTTTTGCTCATT
TTACCGTCGTCTTGAGCAAATATCCCATGATTTGCATCATATGCATTTTGTAGCCCGAATCTTGAAAAGTGC
TCTTTTCAGGATCGTGCCATTTTTGCTCATTTTACCGTCGTCTTGAGCAAATATCCCATGATTTGCATCAAT
ACATGAGAACATAACCACAGTGTCGACCCGCGGAAAAATTCGAGTTTTATGTTGCATTTTGTAGCCCGAATC
TTGAAAAGTGCTCTTTTCAGGATCGTGCCATTTTTGCTCATTTTACCGTCGTCTTGAGCAAATATCCCATGA
TTTGCATCAATACATGAGAACGTCGACCCGCGGCATATGCTCGACAACCCTTAATATAACTTCGTATAATGT
ATGCTATACGAAGTTATTAGGTCTAGAGATCTGTTTAGCTTGCCTCGTCCCCGCCGGGTCACCCGGCCAGCG
ACATGGAGGCCCAGAATACCCTCCTTGACAGTCTTGACGTGCGCAGCTCAGGGGCATGATGTGACTGTCGCC
CGTACATTTAGCCCATACATCCCCATGTATAATCATTTGCATCCATACATTTTGATGGCCGCACGGCGCGAA
GCAAAAATTACGGCTCCTCGCTGCAGACCTGCGAGCAGGGAAACGCTCCCCTCACAGACGCGTTGAATTGTC
CCCACGCCGCGCCCCTGTAGAGAAATATAAAAGGTTAGGATTTGCCACTGAGGTTCTTCTTTCATATACTTC
CTTTTAAAATCTTGCTAGGATACAGTTCTCACATCACATCCGAACATAAACAACCATGGGTAGGAGGGCTTT
TGTAGAAAGAAATACGAACGAAACGAAAATCAGCGTTGCCATCGCTTTGGACAAAGCTCCCTTACCTGAAGA
GTCGAATTTTATTGATGAACTTATAACTTCCAAGCATGCAAACCAAAAGGGAGAACAAGTAATCCAAGTAGA
CACGGGAATTGGATTCTTGGATCACATGTATCATGCACTGGCTAAACATGCAGGCTGGAGCTTACGACTTTA
CTCAAGAGGTGATTTAATCATCGATGATCATCACACTGCAGAAGATACTGCTATTGCACTTGGTATTGCATT
CAAGCAGGCTATGGGTAACTTTGCCGGCGTTAAAAGATTTGGACATGCTTATTGTCCACTTGACGAAGCTCT
TTCTAGAAGCGTAGTTGACTTGTCGGGACGGCCCTATGCTGTTATCGATTTGGGATTAAAGCGTGAAAAGGT

TGGGGAATTGTCCTGTGAAATGATCCCTCACTTACTATATTCCTTTTCGGTAGCAGCTGGAATTACTTTGCA
TGTTACCTGCTTATATGGTAGTAATGACCATCATCGTGCTGAAAGCGCTTTTAAATCTCTGGCTGTTGCCAT
GCGCGCGGCTACTAGTCTTACTGGAAGTTCTGAAGTCCCAAGCACGAAGGGAGTGTTGTAAAGAGTACTGAC
AATAAAAAGATTCTTGTTTTCAAGAACTTGTCATTTGTATAGTTTTTTTATATTGTAGTTGTTCTATTTTAA
TCAAATGTTAGCGTGATTTATATTTTTTTTCGCCTCGACATCATCTGCCCAGATGCGAAGTTAAGTGCGCAG
AAAGTAATATCATGCGTCAATCGTATGTGAATGCTGGTCGCTATACTGCTGTCGATTCGATACTAACGCCGC
CATCCAGTTTAAACGAGCTCTCGAGAACCCTTAATATAACTTCGTATAATGTATGCTATACGAAGTTATTAG
GTGATATCGGATCCAAGCTTCAGCTGAGCTCAGATCTTTCTGCGGCCGCCAGTGGAACTTTGTACGTCCAAA
ATTGAATGACTTGGCCAACTACACTAAGTTCCAGGGCAAAAGTGATTGCCCAAGAAAACCAATACATGTAAC
CATTGGCCGCACCAAATGCTGGAGAAAGGAATCTTTGTGAGAAAACTGTGAAAGAGGATGTAACAGGGATGA
ATGTAGCCATTTCACCCAAGGACTGCGTGACAGAATATGCCAAAGAACCCATAAATAAATATGATATAAGAG
CGCCCACTGGGCCGGCGTTGGTCAGAGGTGTGGATAAACCAATGAAAAGACCTGTACCAATAGTACCACCAA
GGGCAATCATACCGGTTATAAGGGATTTTGCCGATTTCGGCCTATTGGTTAAAAAATGAGCTGATTTAACAA
AAATTTAACGCGAATTTTAACAAAATATTAACGTTTACAATTTCAGGTGGCACTTTTCGGGGAAATGTGCGC
GGAACCCCTATTTGTTTATTTTTCTAAATACATTCAAATATGTATCCGCTCATGAGACAATAACCCTGATAA
ATGCTTCAATAATATTGAAAAAGGAAGAGTATGAGTATTCAACATTTCCGTGTCGCCCTTATTCCCTTTTTT
GCGGCATTTTGCCTTCCTGTTTTTGCTCACCCAGAAACGCTGGTGAAAGTAAAAGATGCTGAAGATCAG

Determination of Flux Control Coefficients from double modulation experiments

The data from Figures 3, 4 and 9 were used to estimate the flux control coefficients of several translation factors. To accomplish this, data for each double modulation were fit to the function:

$$J = \frac{J_{max} \cdot x^n \cdot y^n}{\left(a^n + x^n\right) \cdot \left(b^n + y^n\right)} \tag{1}$$

where J is the flux, x and y are the two modulated factors, and J_{max}, a, and b are two fitting parameters. When properly fit, this function approximates the data from each double modulation experiment, but no special meaning is assigned to it or its parameter values. Instead, we use it simply to estimate the value of the control coefficients, which are partial derivatives of this function. This provides a more robust estimate than simply calculating the slope of the curve by using the data (which would form a crude way of applying finite differences). Recalling that a flux control coefficients of factors x and y are expressed as

$$\begin{aligned} C_x^J &= \frac{dJ / J}{dx / x}, \\ C_y^J &= \frac{dJ / J}{dy / y}, \end{aligned} \tag{2}$$

then using (1) and (2) we obtain:

$$\begin{aligned} C_x^J &= \frac{n \cdot a^n}{\left(a^n + x^n\right)}, \\ C_y^J &= \frac{n \cdot b^n}{\left(b^n + y^n\right)}. \end{aligned} \tag{3}$$

We can therefore estimate the flux control coefficients of each factor involved in the dual modulations, which we do for the reference state (100% of each factor, corresponding to the wildtype).

eIF1 / eIF5

Data relating to Figure 2C and Supporting Fig. 2C.

Best fit parameters:

J_{max}=101.549 a=33.7673 b=29.5722 n=4.14055

$C_{eIF1}^J = 0.046, C_{eEIF5}^J = 0.027$

eIF1 / Pab1

Data relating to Figure 2D and Supporting Fig. 2D.

Best fit parameters:

J_{max}=101.323 a=22.9375 b=37.034 n=3.96484

$C^J_{eIF1} = 0.016, C^J_{Pab1} = 0.076$

eEF1A / eIF4E

Data relating to Figure 5A, C.

Best fit parameters:

J_{max}=663.637 a=1139.38 b=26.7552 n=0.529134

$C^J_{eEF1A} = 0.41, C^J_{eIF4E} = 0.18$

eEF1A / eRF1

Data relating to Figure 5E, G.

Best fit parameters:

J_{max}=106.563 a=34.2909 b=22.8072 n=2.34329

$C^J_{eEF1A} = 0.18, C^J_{eRF1} = 0.071$

Summary

Factor	Flux control coefficient
eIF1	0.031*
eIF5	0.027
Pab1	0.076
eEF1A	0.30*
eIF4E	0.18
eRF1	0.071

* These values obtained as average of the two independent determinations

Supplementary Table 1
***S.cerevisiae* strain construction to top up (enhance) expression of selected genes**

Genes of translation factors with promoter substitutions:	**Top-up for P_{tetO7} promoter**		**Top-up for P_{CTR1}**
	integrated into *lys2* locus (with *BLE* marker)	on a *URA3* plasmid	integrated into *can1* locus (with *HIS5* marker)
P_{tetO7}*SUI1* P_{CuRE3}*TIF5*	P_{HYP2}-21utr*SUI1*	P_{LEU4} *SUI1*	P_{HYP2}*TIF5*
			none
		none	P_{HYP2}*TIF5*
			none
P_{tetO7}*SUI1* P_{CuRE4}*PAB1*	P_{EFT1}-21utr*SUI1*	*none*	P_{HYP2}*PAB1*
			none
	P_{HYP2}-21utr*SUI1*	*none*	P_{HYP2}*PAB1*
			none
	none	P_{TRP1}*SUI1*	P_{HYP2}*PAB1*
			none
	P_{TEF2} promoter substituted with:		
P_{tetO7}*TEF1* P_{CuRE3}*SUP45*	P_{HYP2} promoter with *HIS5* marker- P_{HYP2}*::HIS5TEF2*	none	none
P_{tetO7}*TEF1* P_{CuRE3}*CDC33*	P_{HYP2} promoter, *HIS5* marker removed - P_{HYP2}*TEF2*	P_{DED1}utr*TEF2*	P_{HYP2}*CDC33*
		none	
	P_{HYP2} promoter with *HIS5* marker- P_{HYP2}*::HIS5TEF2*	P_{DED1}utr*TEF2*	none
		none	

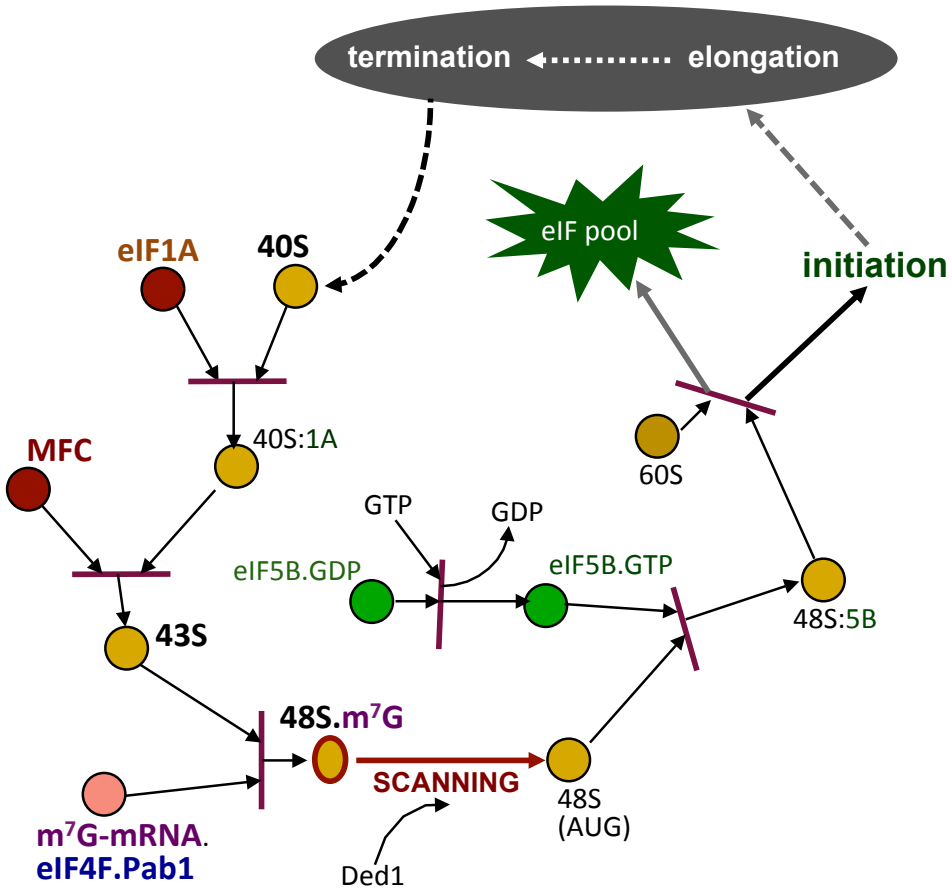
termination
elongation
eIF pool
initiation
eIF1A
40S
40S:1A
MFC
60S
GTP
GDP
eIF5B.GDP
eIF5B.GTP
48S:5B
43S
48S.m7G
SCANNING
48S
(AUG)
m7G-mRNA.
eIF4F.Pab1
Ded1

Graphical Abstract

Translation of a reading frame on eukaryotic mRNA is preceded by a poorly understood scanning process in which a subset of translation factors helps guide ribosomes to the start codon. We use novel experimental and computational tools to study the control status of this scanning step that sits between recruitment of the small ribosomal subunit to the m^7GpppG-capped-5'end of mRNA and the downstream phases of polypeptide initiation, elongation and termination.